Study of phase diagrams for spin-1 Bose-Einstein Condensate under harmonic confinement

A Thesis

submitted to
Indian Institute of Science Education and Research Pune
in partial fulfillment of the requirements for the
BS-MS Dual Degree Programme

by

Sahil Satapathy

Indian Institute of Science Education and Research Pune
Dr. Homi Bhabha Road,
Pashan, Pune 411008, INDIA.

May, 2025

Supervisor: Prof. Arijit Bhattacharyay

Certificate

This is to certify that this dissertation entitled "*Study of phase diagram for spin-1 Bose Einstein Condensate under harmonic confinement*" towards the partial fulfilment of the BS-MS dual degree programme at the Indian Institute of Science Education and Research, Pune represents study/work carried out by Sahil Satapathy at Indian Institute of Science Education and Research under the supervision of Prof. Arijit Bhattacharyay, Department of Physics, during the academic year 2024-2025.

Prof. Arijit Bhattacharyay

Committee:

Prof. Arijit Bhattacharyay

Prof. Rejish Nath

This thesis is dedicated to my family.

Declaration

I hereby declare that the matter embodied in the report entitled " *Study of phase diagram for spin-1 Bose Einstein Condensate under harmonic confinement* " are the results of the work carried out by me at the Department of Physics , Indian Institute of Science Education & Research (IISER) Pune, under the supervision of Prof. Arijit Bhattacharyay, and the same has not been submitted elsewhere for any other degree. Wherever others contribute, every effort is made to indicate this clearly, with due reference to the literature and acknowledgement of collaborative research and discussions.

Sahil Satapathy

Sahil Satapathy

20201249

Acknowledgments

I sincerely thank my supervisor, Dr. Arijit Bhattacharyay, for his invaluable guidance, encouragement, and support throughout my thesis. His expertise and insights have been instrumental in shaping this thesis. In addition to his exceptional scientific prowess, he embodies a remarkable personality, and I consider myself fortunate enough to have had the opportunity to work under his guidance.

I thank my TAC, Dr. Rejish Nath, for giving precious suggestions.

A special thanks to Dr. Projjwal Kanti Kanjilal, doctoral fellow and IISER Pune alumni, for his invaluable insights regarding the topic during my project. I have had many fruitful discussions with him, greatly benefiting my research.

I would also like to thank my friends and family for their constant support and encouragement throughout this journey.

Finally, I want to thank the Director of IISER Pune and the Dean (Graduate Studies) of IISER Pune for the excellent facilities at the institute that helped me pursue this project.

Contents

List of Tables

List of Figures

Abstract

In this thesis, we discuss a variational method that can help us to accurately determine the density profile of both single-component and multi-component ground states for a Spinor-Bose-Einstein condensate confined in a harmonic potential. Subsequently, we will apply our variational method to determine the phase boundary for a spin-1 Bose-Einstein condensate in a quasi-one-dimensional harmonic confinement. We begin by finding energy and number densities for all possible stationary states under the Thomas-Fermi approximation. Although the Thomas-Fermi approximation works better for larger condensates, it can fail even for larger condensates when the difference in energy between the competing ground states is minimal. Because of these limitations of Thomas-Fermi, researchers started exploring more accurate methods, such as numerical simulations, to determine the density profile of ground states for condensates under confinement. However, numerical simulations prove to be computationally expensive in higher dimensions. Thus, there is a growing need for analytical methods to efficiently and accurately determine the density profile of ground states for condensate under confinement and subsequently determine the phase boundary. This is where our variational method proves particularly effective. Furthermore, accurately finding the exact location of the phase boundary for a trapped system is crucial for studying critical phenomena like phase transitions, quench-induced dynamics, etc.

Chapter 1

Introduction

1.1 Bose-Einstein Condensation

In 1924, physicist Satyendra Nath Bose integrated the light quantum hypothesis with statistical mechanics to obtain Planck's formula and sent his findings to Einstein. Recognizing the significance of Bose's work, Einstein submitted the manuscript on his behalf to Zeitschrift für Physik [4]. Einstein then extended this theory to other particles [7], notably the monoatomic ideal gas, and the result was the emergence of Bose-Einstein statistics, which dictates the behavior of Bose gas. In the following year, Einstein predicted that at exceedingly lower temperatures, as the de Broglie wavelength of atoms becomes comparable to the interatomic separation, the ideal gas of bosons undergo condensation into the ground state with the lowest energy, leading to the formation of Bose-Einstein Condensates (BEC) [29].

It was in the year 1938 that Fritz London [21] proposed Bose-Einstein condensation as the underlying mechanism behind of phenomenon super-fluidity in Helium. Later, in 1947, Bogoliubov [3] introduced his new perturbative approach to show the effects of interaction on BECs in realistic samples. In 1956, Oliver Penrose and Lars Onsager [24] further generalized the mathematical formalism of BEC in the presence of interaction [16]. Four years later, In 1960, Lev Pitaevskii [23] and Eugene Gross [10] independently developed the mean-field theory, which marked a significant advancement in the theoretical understanding of this field. Their works demonstrated that, due to macroscopic occupation of the ground state, a BEC can be represented by a semi-classical wave function (order parameter), and the resulting governing equation is called the Gross-Pitaevskii (G-P) equation.

Bose-Einstein Condensates form at extremely low temperatures (about nano-kelvin (nK)). These days, There exist various cooling techniques used to achieve such temperatures,

- **Laser cooling technique** [2][11]: This method uses carefully tuned lasers to cool down

atoms. However, this method can only cool atoms to milli- Kelvin (mK) range.

- **Evaporative cooling** [22]: This technique is quite similar to how a cup of coffee (for example) cools down[16], where the higher energy-carrying molecules leave the cup, and remaining molecules redistribute energy to lower the temperature of the system.

- Further, to enhance this method, a radioactive frequency field is applied, which helps the high-energy particles to escape. However, one drawback is the significant loss of trapped particles. But this limitation could be avoided using a dimple trap [28], where the introduction of a tightly focused red-de tuned laser beam creates a localized potential inside the broader trapping potential. A dimple trap is a highly focused optical potential superimposed on a larger trap, increases atomic density and improves cooling efficiency [28].

In 1995, Eric Cornell and Carl Wieman[1] observed BEC for the first time by using 3000 atoms of ^{87}Rb and achieved a transition temperature of around 170 nK (In this sample, the constituent atoms were in a single spin state, making it a scalar BEC) within a magnetic trap [12]. A few months later, Wolfgang Ketterle successfully produced BEC with ^{23}Na particles [6] and in the same year ^{7}Li was also Bose-condensed [5].

1.2 Spinor Bose-Einstein Condensates

The magnetic trapping enables the formation of Bose-Einstein Condensates only with atoms in low field-seeking hyperfine projections [8] [19]. Consequently, all constituent atoms in the Bose-Einstein Condensate remain in a single spin state. However, suppose one traps the condensate that does not energetically favor a single spin state. In that case, the spin degrees of freedom alongside varying density can lead to a richer system [16]. This is achieved by using an optical trap [25, 27]. Such BECs with spin internal degrees of freedom are known as Spinor Bose-Einstein Condensate. In contrast, a Bose-Einstein Condensate lacking spin degrees of freedom is often called a Scalar Bose-Einstein Condensate. In the year 1998, Spinor Bose-Einstein Condensate was first reported by using spin-1 ^{23}Na atoms confined in an optical dipole trap [25], paving the way for a new frontier to research in ultra-cold atomic systems. Note that, for a spin-f BEC, the order parameter(wave function) will have $2f+1$ components [25, 26], which can vary spatially and temporally, gives rise to various spin textures.

In the following, we discuss some known essential theoretical aspects of spin-1 BEC. The contents of the following section are based mainly on the review article by Yuki Kawaguchi and Masahito Ueda [18] and the PhD Thesis of Projjwal Kanti Kanjilal [16], which have been the motivation for the work done and presented in this thesis.

1.2.1 Hamiltonian for spinor BEC

The second-quantized Hamiltonian, in terms of density field operators, comprises interacting and non-interacting components.

$$\hat{H} = \hat{H}_0 + \hat{H}_{int} \tag{1.1}$$

Non-interacting components of Hamiltonian include the kinetic energy term, trapping potential $U_{trap}(r)$, linear and quadratic Zeeman terms [16, 18] respectively,

$$\hat{H}_0 = \int dr \sum_{m',m=0,1,-1} \hat{\Psi}_m^\dagger \left[\frac{-\hbar^2\nabla^2}{2M} + U_{trap}(r) - p(f_z)_{mm'} + q(f_z^2)_{mm'} \right] \hat{\Psi}_{m'}. \tag{1.2}$$

In the above expressions, M denotes the boson's mass undergoing condensation. The confining potential is denoted by $U_{trap}(r)$, and the field operator corresponding to the m^{th} sub-component is given by $\hat{\Psi}_m$. The f_z represents z-component of the Pauli Spin-1 matrix [18] with matrix elements $(f_z)_{mm'} = (\delta_{mm'})m$ and $(f_z^2)_{mm'} = (\delta_{mm'})m^2$. The parameter p represents the strength of the linear Zeeman effect and is given by $p = -g\mu_B B$, where μ_B denotes the Bohr magneton which is defined by $\frac{e\hbar}{2m_e}$ (where m_e is the electron mass) where g is the Landé g factor. The Quadratic Zeeman term is calculated as the sum of contributions arising from microwave field (q_{MW}) and magnetic field (q_B) i.e. $q = q_{MW} + q_B$. Here $q_B = \frac{g^2\mu_B^2 B^2}{\Delta E_{hf}}$ and $\Delta E_{hf} = E_m - E_i$ denotes the hyperfine splitting energy, calculated as the difference between the intermediate energies(E_m) and initial energy(E_i). Furthermore, the ability to tune the value of q_{MW} independent of q_B applying an off-resonant linearly polarized microwave field [9, 20], allows one to tune the quadratic (q) and linear (p) Zeeman terms independently [16].

The interacting component of Hamiltonian is given by

$$\hat{H}_{int} = \frac{1}{2}\int dr \left(c_0 : \hat{n}^2(r) : + c_1 : \hat{\mathbf{F}}^2(r) : \right). \tag{1.3}$$

The notation ': :' in the above eqn.(1.3) denotes the usual normal ordering, which places creation operators to the left of annihilation operators. In this context, c_0 represents the spin-independent interaction coefficient and c_1 represents the spin-dependent interaction coefficient [14, 16] as

$$c_0 = \left(\frac{2a_2 + a_0}{3} \right) \frac{4\pi\hbar^2}{M} \quad and \quad c_1 = \left(\frac{a_2 - a_0}{3M} \right) 4\pi\hbar^2. \tag{1.4}$$

The $\hat{n}$ denotes the number density operator and $\hat{F}_i$ represents components of spin density operators [16, 18]

$$\sum_{m=-1}^{1} \hat{\Psi}_m^\dagger(r)\hat{\Psi}_m(r) = \hat{n}(r), \tag{1.5}$$

$$\sum_{m',m=-1}^{1} (f_i)_{mm'} \hat{\Psi}^{\dagger}_{m}(r)\hat{\Psi}_{m'}(r) = \hat{F}_i, \tag{1.6}$$

where f_i(i=z,x,y) are Pauli Spin-1 matrices given by [18]

$$\frac{1}{\sqrt{2}}\begin{bmatrix} 0 & 1 & 0 \\ 1 & 0 & 1 \\ 0 & 1 & 0 \end{bmatrix} = f_x \quad , \quad \frac{i}{\sqrt{2}}\begin{bmatrix} 0 & -1 & 0 \\ 1 & 0 & -1 \\ 0 & 1 & 0 \end{bmatrix} = f_y \quad and \quad \begin{bmatrix} 1 & 0 & 0 \\ 0 & 0 & 0 \\ 0 & 0 & -1 \end{bmatrix} = f_z. \tag{1.7}$$

1.2.2 Mean-Field Theory and Gross-Pitaevskii Equation for spinor BEC

Mean field theory is generally derived by substituting the field operators with their expectation values. To develop it, we begin by expanding the field operators as

$$\hat{\Psi}_m(r) = \sum_i \hat{a}_{mi}\phi_{mi}(r) \tag{1.8}$$

where $\phi_{mi}(r)$ denotes the complete set of orthonormal basis functions that describes the spatial mode i with magnetic quantum number m [18]. The $\hat{a}_{mi}$ which satisfies canonical commutation relations represent corresponding bosonic annihilating operators

$$[\hat{a}^{\dagger}_{m'j}, \hat{a}_{mi}] = \delta_{ij}\delta_{mm'} \quad and \quad [\hat{a}_{m'j}, \hat{a}_{mi}] = [\hat{a}^{\dagger}_{m'j}, \hat{a}^{\dagger}_{mi}] = 0. \tag{1.9}$$

The mean-field approximation assumes all the bosons occupy a single spin state and spatial mode (i.e., $i = 0$). Thus, the state vector is expressed as

$$|\xi\rangle = \frac{1}{\sqrt{N!}}\left(\sum_{m=-1}^{1} \xi_m \hat{a}^{\dagger}_{m0}\right)^N |vac\rangle \tag{1.10}$$

here $|vac\rangle$ represents the particle vacuum and ξ_m follows the normalization condition i.e. $\sum_{m=-1}^{1} |\xi_m|^2 = 1$. Considering the order parameter $\psi_m(r) = \sqrt{N}\xi_m\phi_{m0}(r)$, it is easy to show that [16],

$$\langle\xi|\hat{\Psi}_m(r_2)|\xi\rangle = \langle\xi|\hat{\Psi}^{\dagger}_m(r_2)|\xi\rangle = 0 \tag{1.11}$$

$$\langle\xi|\hat{\Psi}^{\dagger}{}_m(r_1)\hat{\Psi}_{m'}(r_2)|\xi\rangle = \psi^*_m(r_1)\psi_{m'}(r_2) \tag{1.12}$$

$$\langle\xi|\hat{\Psi}^{\dagger}_{m_1}(r_1)\hat{\Psi}^{\dagger}_{m_2}(r_2)\hat{\Psi}_{m_3}(r_3)\hat{\Psi}_{m_4}(r_4)|\xi\rangle = \left(1-\frac{1}{N}\right)\psi^*_{m_1}(r_1)\psi^*_{m_2}(r_2)\psi_{m_3}(r_3)\psi_{m_4}(r_4) \tag{1.13}$$

Utilizing the mean-field approximation, the Hamiltonian in eqn.(1.1) is replaced with its ex-

pectation value. Furthermore, ignoring the terms of order 1/N, we get

$$\langle\xi|\hat{H}|\xi\rangle = E[\psi] = \int dr \left[\sum_{m,m'=-1}^{1} \psi_m^*(r) \left(-\frac{\hbar^2\nabla^2}{2M} + qm^2 - pm + U_{trap}(r) \right) \psi_m(r) + \frac{c_0}{2} n^2(r) + \frac{c_1}{2} |\mathbf{F}(r)|^2 \right] \tag{1.14}$$

Herein, $n(r)$ denotes particle number density and $\mathbf{F}(r)$ signifies spin density expectation value and are represented by

$$n(r) = \langle\xi|\hat{n}(r)|\xi\rangle = \sum_{m=-1}^{1} \psi_m^*(r)\psi_m(r), \tag{1.15}$$

$$F_i = \langle\xi|\hat{F}_i(r)|\xi\rangle = \sum_{m,m'=-1}^{1} \psi_m^*(f_i)_{mm'}(r)\psi_{m'}(r), \tag{1.16}$$

where $(f_i)_{mm'}$ denotes the mm' element of the Pauli spin-1 matrices (eqn. 1.7).

Observe that the dynamics of mean-field are governed by,

$$i\hbar\frac{\partial\psi_m}{\partial t} = \frac{\delta E}{\delta\psi_m^*(r)}. \tag{1.17}$$

Using eqn.(1.14) in the above relation gives us,

$$i\hbar\frac{\partial\psi_m}{\partial t} = \left(-\frac{\hbar^2\nabla^2}{2M} + qm^2 - pm + U_{trap}(r) \right) \psi_m(r,t) + c_0 n(r,t)\psi_m(r,t) + c_1 \sum_{m'=-1}^{1} \mathbf{F}(r,t).f_{mm'}\psi_{m'}(r,t). \tag{1.18}$$

This above equation is a multi-component time-dependent GP equation where $m = -1, 0, +1$.

1.2.3 Stationary States in absence of confinement

We can express the time-dependent wave function as a product of space-dependent and time-dependent functions,

$$\psi_m(r,t) = \psi_m(r)\, exp(-\frac{i\mu t}{\hbar}) \tag{1.19}$$

here, μ denotes the chemical potential.
Substituting eqn.(1.19) in eqn.(1.18) would give us three coupled time-independent GP (TIGP) equations,

$$\frac{c1}{\sqrt{2}}F_{-}(r)\psi_0(r) + \left(-\frac{\hbar^2\nabla^2}{2M} + q - p + U_{trap}(r) + c_0 n(r) + c_1 F_z(r) - \mu\right)\psi_1(r) = 0 \tag{1.20}$$

$$\psi_0(r)\left(-\frac{\hbar^2\nabla^2}{2M} + c_0 n(r) + U_{trap}(r) - \mu\right) + + \frac{c1}{\sqrt{2}}\psi_1(r)F_{+}(r) + \frac{c1}{\sqrt{2}}\psi_{-1}(r)F_{-}(r) = 0 \tag{1.21}$$

$$\psi_{-1}(r)\left(-\frac{\hbar^2}{2}\frac{\nabla^2}{M} + q + p + U_{trap}(r) + c_0 n(r) - c_1 F_z(r) - \mu\right) + \frac{c1}{\sqrt{2}}F_{+}(r)\psi_0(r) = 0 \tag{1.22}$$

where $F_{\pm 1}(r) = F_x(r) \pm iF_y(r)$ and,

$$\frac{1}{\sqrt{2}}\left[\psi_0(r)\psi_1^*(r) + \psi_{-1}^*(r)\psi_0(r) + (\psi_{-1}(r) + \psi_1(r))\,\psi_0^*(r)\right] = F_x(r) \tag{1.23}$$

$$\frac{i}{\sqrt{2}}\left[-\psi_1^*(r)\psi_0(r) + \psi_0^*(r)\,(\psi_1(r) - \psi_{-1}(r)) + \psi_0(r)\psi_{-1}^*(r)\right] = F_y(r) \tag{1.24}$$

$$|\psi_1(r)|^2 - |\psi_{-1}(r)|^2 = F_z(r) \tag{1.25}$$

From this point onward, solving the above TIGP equations helps us to obtain the feasible stationary states and their corresponding energies. The most straightforward situation to consider from this point would be to see when there is the absence of trapping potential, i.e., $U_{trap}(r) = 0$ (Homogeneous case). In this scenario, the system exhibits a constant number density function, which allows us to neglect the kinetic energy. This system is solved exclusively in [18], and we will state the results. For this case, we would observe five different stationary states, namely Ferromagnetic(F1) or (1,0,0) state where only $m = 1$ level is filled, Ferromagnetic(F2) or (0,0,1) state where only $m = -1$ level is filled, Polar(P) or (0,1,0) state where only $m = 0$ level is filled, Antiferromagnetic (AF) or (1,0,1) state where both $m = 1$ and $m = -1$ levels are filled and (1,1,1) state where all the spin projections ($m = 0, -1, +1$) are filled.

In the phase diagram (Fig.1.1), different stationary states are F1 or Ferromagnetic or (1,0,0) state, F2 or Ferromagnetic or (0,0,1) state,Antiferromagnetic state or (1,0,1) state, Polar state or (0,1,0) state and (1,1,1) state. Observe that, for condensates with the antiferromagnetic type of spin interaction i.e., $c_1 > 0$, Ferromagnetic, Polar, or Antiferromagnetic states act as the ground state depending on the values of q and p. Similarly, for condensates with the ferromagnetic type of spin interaction i.e., $c_1 < 0$, Polar, (1,1,1) state or any of the Ferromagnetic states becomes the ground state depending on q and p. Furthermore, for condensates with no spin-spin interaction ($c_1 = 0$),

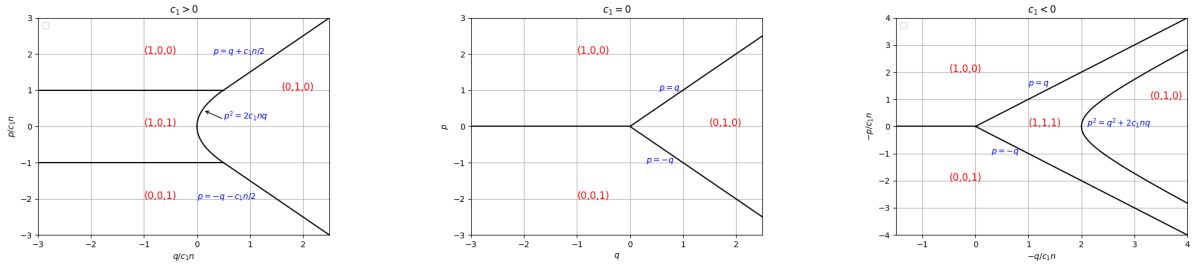

(a) $c_1 > 0$ (b) $c_1 = 0$ (c) $c_1 < 0$

Figure 1.1: phase diagram for spin-1 condensate in the absence of any trapping potential

the system ground state can either be Polar state or ferromagnetic depending on q and p.

In Chapter 2, we will focus on realistic situations of the condensate under harmonic confinement. Unlike the homogeneous case, where the number density is considered a constant function, a trapped condensate would exhibit a spatially varying number density profile because the trapping geometry would dictate the condensate's number density.

Chapter 3 will present a Variational approach that would help us accurately determine the number density profile for ground states of a Spinor Bose-Einstein Condensate in harmonic confinement.

In Chapter 4, we will use the variational method to construct phase boundaries for a confined condensate and analyze the deviations from the homogeneous case. Furthermore, we will establish universal (collapsed) phase boundaries independent of the number of condensate particles (N).

Chapter 2

Stationary States in presence of trapping

In the previous chapter, we saw the results for Spinor Bose-Einstein condensate in the absence of trapping potential. However, in a practical setting, a Bose-Einstein Condensate is confined within a potential, which is typically harmonic. Consequently, unless this confining potential is turned off, trapping effects cannot be neglected. As a result, the constant number density assumption, which was valid for homogeneous cases, no longer holds for trapped condensate. The trapping geometry directly influences the condensate's number density. Solving the Gross-Pitaevskii equation in this scenario is challenging due to its nonlinear nature and the presence of derivatives.

This chapter begins with investigating the condensate in a generic confining potential. We apply the Thomas-Fermi(T-F) approximation, generally applicable for high-density condensates, where kinetic energy is omitted due to its minimal contribution compared to interaction energy. We would use this approximation to determine the energy and number densities associated with individual stationary states. Our next task would be to look at a previously established Variational method used in similar contexts. The contents of this section are mostly taken from a PhD Thesis by Projjwal Kanti Kanjilal [16]

2.1 Stationary States in Presence of a Confining Potential

As we observed earlier, the ansatz to use in the absence of trapping was eqn(1.19), but in the presence of a trapping potential, the ansatz to follow is [16]

$$\sqrt{n_m(r)}\,.\,exp(-i\theta_m).exp(-\frac{i\mu t}{\hbar}) = \psi_m(r,t). \tag{2.1}$$

where $n_m(r)$ refers to the number density of the m^{th} sub-component. Here, stationary state refers to the stationarity of $n_m(r)$. Further, the spatial dependence of θ_m is neglected because any such dependency will cause velocity, which will be against the stationarity of phase [16].

Substituting the above ansatz in eqn.(1.18) and then equating the imaginary parts separately for different spin projections(i.e., $m = -1, 0, +1$) would give us the evolution equations for different sub-component number densities [16]

$$\dot{n_0}(r) = -\frac{4n_0\sqrt{n_{-1}n_1}\ c_1 \sin\theta_r}{\hbar} \tag{2.2}$$

$$\dot{n}_{\pm 1}(r) = \frac{2n_0\sqrt{n_{-1}n_1}\ c_1 \sin\theta_r}{\hbar} \tag{2.3}$$

where θ_r refers to the relative phase, and is given by $\theta_{-1} + \theta_1 - 2\theta_0 = \theta_r$.

Similarly, equating the real parts separately for different spin projections(i.e., $m = -1, 0, +1$) would result in phase dynamics equations.

$$\hbar\dot{\theta}_0 = c_1(n_{-1} + n_1 + 2\sqrt{n_1 n_{-1}}\cos\theta_r) + \frac{1}{\sqrt{n_0(r)}}\left(-\frac{\hbar^2\nabla^2}{2.M} + U_{trap}(r) - \mu + c_0 n\right)\sqrt{n_0(r)}, \tag{2.4}$$

$$\begin{aligned}\hbar\dot{\theta}_1 = \frac{1}{\sqrt{n_1(r)}}&\left(-\frac{\hbar^2}{M}\frac{\nabla^2}{2} - \mu + U_{trap}(r) + c_0 n\right)\sqrt{n_1(r)} + q \\ &+ \frac{c_1 n_0}{\sqrt{n_1(r)}}\left(\sqrt{n_{-1}(r)}\cos\theta_r + \sqrt{n_1(r)}\right) - c_1(n_{-1} - n_1) - \ p,\end{aligned} \tag{2.5}$$

$$\begin{aligned}\hbar\dot{\theta_{-1}} = \frac{1}{\sqrt{n_{-1}(r)}}&\left(-\frac{\hbar^2}{M}\frac{\nabla^2}{2} - \mu + U_{trap}(r) + c_0 n\right)\sqrt{n_{-1}(r)} + q \\ &+ \frac{c_1 n_0}{\sqrt{n_{-1}(r)}}\left(\sqrt{n_1(r)}\cos\theta_r + \sqrt{n_{-1}(r)}\right) + c_1(n_{-1} - n_1) + \ p.\end{aligned} \tag{2.6}$$

Using the same ansatz (eqn. (2.1)) we can also simplify the energy expression(eqn. (1.14)) as

$$\begin{aligned}E &= \int e(r)dr \\ &= \int dr\left[\sum_{m=0,-1,1}\left(-\sqrt{n_m(r)}\frac{\hbar^2}{M}\frac{\nabla^2}{2}\sqrt{n_m(r)} + U_{trap}(r)n_m(r)\right) + n_1(q-p) + n_{-1}(p-q) + \right. \\ &\quad \left. + \frac{c_0.n^2(r)}{2} + c_1 n_0(n_{-1} + n_1 + 2\cos\theta_r\sqrt{n_{-1}n_1}) + \frac{c_1.(n_1 - n_{-1})^2}{2}\right],\end{aligned} \tag{2.7}$$

here e(r) refers to the energy density. From this point onward, we would solve eqn.(2.4) - eqn.(2.6) to obtain a complete description of the stationary states under confinement.

2.1.1 Single-component states

A single component state is a stationary state where two sub-components are empty while the remaining sub-component is populated. In the context of the spin-1 case, there are three possible single-component states. The first one is the Polar state denoted by (0,1,0). The remaining 2 being ferromagnetic states denoted by F1 or (1,0,0) and F2 or(0,0,1)

Ferromagnetic or F1 or (1,0,0) state

F1 state corresponds to empty $m = -1, 0$ levels and populated $m = 1$ level , i.e. $n_0 = n_{-1} = 0$ and $n_1(r) = n(r)$, where n(r) represents the total number density. For this state, the phase equation for $\dot{\theta}_1$ is set to 0 ($\hbar\dot{\theta}_1 = 0$).

$$-\frac{\hbar^2}{M}\frac{\nabla^2}{2} - p + c_0 n(r) + U_{trap}(r) \; + c_1 n(r) + q - \mu = 0. \tag{2.8}$$

Thomas-Fermi(T-F) approximation

The Thomas-Fermi approximation, applicable to condensates with a high density of particles, relies on the assumption that the interaction energy is significantly greater than the kinetic energy. As a result, the kinetic energy is ignored, and the number density function we get is

$$n_1(r) = \frac{\mu + p - q - U_{trap}(r)}{c_0 + c_1} = n(r). \tag{2.9}$$

Furthermore the energy density of F1 state is calculated by substituting eqn.(2.9) in eqn.(2.7) which would give us [16],

$$e_{F1}^{TF}(r) = (U_{trap}(r) + q - p)\left(\frac{\mu - U_{trap}(r) - q + p}{c_1 + c_0}\right) + \frac{(\mu - U_{trap}(r) - q + p)^2}{2(c_1 + c_0)}. \tag{2.10}$$

Ferromagnetic or F2 or (0,0,1) state

F2 state corresponds to empty $m = 1, 0$ level and populated $m = -1$ level , i.e. $n_0 = n_1 = 0$ and $n(r) = n_{-1}(r)$. The phase equation for $\dot{\theta}_{-1}$ is set to 0 for this state.

$$-\frac{\hbar^2}{M}\frac{\nabla^2}{2} + p + c_0 n(r) + U_{trap}(r) \; + c_1 n(r) + q - \mu = 0. \tag{2.11}$$

Under the Thomas-Fermi approximation, the number density function becomes

$$n_{-1}(r) = \frac{\mu - U_{trap}(r) - q - p}{c_0 + c_1} = n(r). \tag{2.12}$$

Finally, the energy density of F2 state is calculated by substituting eqn.(2.12) in eqn.(2.7), which would give us [16],

$$e_{F2}^{TF}(r) = (U_{trap}(r) + q + p)\left(\frac{\mu - U_{trap}(r) - q - p}{c_1 + c_0}\right) + \frac{(\mu - U_{trap}(r) - q - p)^2}{2(c_1 + c_0)}. \tag{2.13}$$

Polar state or (0,1,0) state

Polar state corresponds to empty $m = 1, -1$ level, i.e. $n_{-1} = n_1 = 0$ and populated $m = 0$ level, i.e. $n_0(r) = n(r)$. The phase equation for $\dot{\theta_0}$ is set to 0 for this state. The number density function for the polar state under the T-F approximation becomes

$$n(r) = n_0(r) = \frac{\mu - U_{trap}(r)}{c_0}. \tag{2.14}$$

Using eqn.(2.14) in eqn.(2.7) would give us the energy density of Polar state [16],

$$e_{pol}^{TF} = U_{trap}(r)\left(\frac{\mu - U_{trap}(r)}{c_0}\right) + \frac{(\mu - U_{trap}(r))^2}{2c_0}. \tag{2.15}$$

2.1.2 Multi-component states

A multi-component state is a stationary state where two or more sub-components are populated. In the context of the spin-1 case, there are five possible multi-component states. There are three stationary states where one sub-component is empty while the remaining two are populated. One state is the Anti-Ferromagnetic state (AF), denoted by (1,0,1). The other two are mixed-ferromagnetic states denoted by (1,1,0) and (0,1,1). The remaining two stationary states are Anti-Phase-matched and Phase-matched states, where all 3 sub-components are populated.

Anti-Ferromagnetic or AF or (1,0,1) state

AF state corresponds to empty $m = 0$ level, i.e. $n_0 = 0$ and populated $m = 1, -1$ level. For this state, the phase equation for $\dot{\theta_1}$ and $\dot{\theta_{-1}}$ are set to 0. Setting $\hbar\dot{\theta_1} = 0$ and under the Thomas-Fermi approximation, we would get

$$U_{trap}(r) + c_0 n - p - c_1(n_{-1} - n_1) + q - \mu = 0. \tag{2.16}$$

Setting $\hbar\dot{\theta_{-1}} = 0$ and under the Thomas-Fermi approximation, we would get

$$(U_{trap}(r) - \mu + c_0 n) + q - c_1(n_1 - n_{-1}) + p = 0. \tag{2.17}$$

Adding eqn.(2.16) and eqn.(2.17) would give us the total number density function as,

$$\frac{\mu - U_{trap}(r) - q}{c_0} = n(r). \tag{2.18}$$

Subtracting eqn.(2.17) from eqn.(2.16), we can get the magnetization as

$$n_1(r) - n_{-1}(r) = \frac{p}{c_1} \tag{2.19}$$

For AF state $n_{-1}(r) + n_1(r) = n(r)$. Using the expressions for magnetization and total number density function, we can calculate the individual sub-component number densities for the AF state as

$$n_1(r) = \frac{\mu - U_{trap}(r) - q}{2c_0} + \frac{p}{2c_1}, \tag{2.20}$$

$$n_{-1}(r) = \frac{\mu - U_{trap}(r) - q}{2c_0} - \frac{p}{2c_1}. \tag{2.21}$$

The corresponding energy density is [16],

$$\begin{aligned} e_{AF}^{TF}(r) &= \frac{c_0}{2} n^2(r) + qn(r) - \frac{p^2}{2c_1} + U_{trap}(r)n(r) \\ &= (U_{trap}(r) + q)\left(\frac{\mu - U_{trap}(r) - q}{c_0}\right) + \frac{(-U_{trap}(r) + \mu - q)^2}{2c_0} - \frac{p^2}{2c_1}. \end{aligned} \tag{2.22}$$

Mixed-Ferromagnetic or MF1 or (1,1,0) state

This stationary state corresponds to empty $m = -1$ level, i.e., $n_{-1} = 0$ and populated $m = 1, 0$ levels. For this state, the phase equation for $\dot{\theta}_1$ and $\dot{\theta}_0$ are set to 0. Setting $\hbar\dot{\theta}_1 = 0$ and under T-F approximation, we get

$$U_{trap}(r) + c_0 n - \mu + c_1 n_1 + q - p + c_1 n_0 = 0, \tag{2.23}$$

and setting $\hbar\dot{\theta}_0 = 0$ with T-F approximation,

$$U_{trap}(r) + c_0 n - \mu + c_1 n_1 = 0. \tag{2.24}$$

For this stationary state, $n_1(r) + n_0(r) = n(r)$. Plugging it in eqn.(2.23), we get total number density as,

$$\frac{\mu - U_{trap}(r) + p - q}{c_1 + c_0} = n(r). \tag{2.25}$$

Subtracting eqn.(2.24) from eqn.(2.23) we get,

$$n_0(r) = \frac{p-q}{c_1}. \tag{2.26}$$

Putting the above total number density expression in eqn.(2.24) would give us,

$$n_1(r) = \frac{\mu + p - U_{trap}(r) - q}{c_1 + c_0} - \frac{p-q}{c_1}. \tag{2.27}$$

Using the above expressions for total number density and individual sub-component densities, we can now find expression for the energy density of this stationary state [16],

$$\begin{aligned} e^{TF}_{MF1}(r) = U_{trap}(r)\left(\frac{\mu + p - U_{trap}(r) - q}{c_1 + c_0}\right) + \frac{c_0}{2}\left(\frac{\mu + p - U_{trap}(r) - q}{c_1 + c_0}\right)^2 \\ + \frac{c_1}{2}\left(\frac{\mu + p - U_{trap}(r) - q}{c_1 + c_0} - \frac{p-q}{c_1}\right)^2. \end{aligned} \tag{2.28}$$

Mixed-Ferromagnetic or MF2 or (0,1,1) state

MF2 state corresponds to empty $m = 1$ level, i.e., $n_1 = 0$ and populated $m = -1, 0$ levels. For this state, the phase equation for $\dot{\theta_0}$ and $\dot{\theta_{-1}}$ are set to 0. Setting $\hbar\dot{\theta_{-1}} = 0$ and under the Thomas-Fermi approximation, we get

$$U_{trap}(r) + c_0 n - \mu + c_1 n_{-1} + q + p + c_1 n_0 = 0, \tag{2.29}$$

and setting $\hbar\dot{\theta}_0 = 0$ under the Thomas-Fermi approximation gives

$$U_{trap}(r) + c_0 n - \mu + c_1 n_{-1} = 0. \tag{2.30}$$

For MF2 state, $n(r) = n_0(r) + n_{-1}(r)$. Plugging it in eqn.(2.29), we get total number density as

$$\frac{\mu - U_{trap}(r) - p - q}{c_1 + c_0} = n(r). \tag{2.31}$$

Then, subtracting eqn.(2.29) from eqn.(2.30) gives

$$n_0(r) = \frac{-p-q}{c_1}. \tag{2.32}$$

Substituting the total number density in eqn.(2.30) would give us,

$$n_{-1}(r) = \frac{\mu - p - U_{trap}(r) - q}{c_1 + c_0} + \frac{q+p}{c_1}. \tag{2.33}$$

Using the above expressions for total number density and individual sub-component densities, we can find the total energy density as [16]

$$e^{TF}_{MF2}(r) = U_{trap}(r)\left(\frac{\mu - p - U_{trap}(r) - q}{c_1 + c_0}\right) + \frac{c_0}{2}\left(\frac{\mu - p - U_{trap}(r) - q}{c_1 + c_0}\right)^2 + \frac{c_1}{2}\left(\frac{\mu - p - U_{trap}(r) - q}{c_1 + c_0} + \frac{q + p}{c_1}\right)^2. \tag{2.34}$$

Phase-Matched or PM or (1,1,1) state with $\theta_r = 0$

PM state corresponds to a state where the relative phase θ_r is zero, and all three sub-components are occupied. For this state, the phase equation for $\dot{\theta_0}$, $\dot{\theta_1}$ and $\dot{\theta_{-1}}$ are all set to 0. Under the Thomas-Fermi approximation, setting $\hbar\dot{\theta_1} = 0$ will give us

$$U_{trap}(r) + c_0 n - \mu - p + q + (\sqrt{n_{-1}} + \sqrt{n_1})\frac{c_1 n_0}{\sqrt{n_1}} = c_1(n_{-1} - n_1). \tag{2.35}$$

Under the same approximation setting $\hbar\dot{\theta_{-1}} = 0$ gives us

$$-c_1(n_1 - n_{-1}) + U_{trap}(r) + c_0 n - \mu + p + q + (\sqrt{n_{-1}} + \sqrt{n_1})\frac{c_1 n_0}{\sqrt{n_{-1}}} = 0' \tag{2.36}$$

and setting $\hbar\dot{\theta_0} = 0$ gives

$$U_{trap}(r) - \mu + c_0 n + c_1(n_{-1} + n_1 + 2\sqrt{n_{-1} n_1}) = 0, \tag{2.37}$$

where for PM state, $n_1(r) + n_{-1}(r) + n_0(r) = n(r)$.

Further, we can solve eqn.(2.35) - eqn.(2.37) to get our total number density and individual sub-component number density (For details one can look at [13, 16])

$$n_1(r) = \frac{q^2 + p^2 + 2pq}{4q^2}\left(n(r) - \frac{p^2 - q^2}{2c_1 q}\right), \tag{2.38}$$

$$n_{-1}(r) = \frac{p^2 + q^2 - 2pq}{4q^2}\left(n(r) - \frac{p^2 - q^2}{2c_1 q}\right), \tag{2.39}$$

$$n_0(r) = \frac{(q^2 - p^2)}{2q^2}\left(n(r) - \frac{q^2 + p^2}{2c_1 q}\right), \tag{2.40}$$

and

$$n(r) = \frac{\mu + \frac{p^2 - q^2}{2q} - U_{trap}(r)}{c_1 + c_0}. \tag{2.41}$$

Finally, using the equations for sub-component number densities and total number density, one can find the expression for energy density [16]

$$e_{PM}^{TF}(r) = U_{trap}(r)\left(\frac{k_2 - U_{trap}(r)}{c_1+c_0}\right) + \frac{c_0}{2}\left(\frac{k_2 - U_{trap}(r)}{c_1+c_0}\right)^2 + \frac{c_1}{2}\left(\frac{k_2 - U_{trap}(r)}{c_1+c_0} - \frac{p^2-q^2}{2qc_1}\right)^2, \tag{2.42}$$

where $k_2 = \mu + \frac{p^2-q^2}{2q}$.

Anti-Phase-matched or APM or (1,1,1) state with $\theta_r = \pi$

APM state corresponds to a state where the relative phase θ_r is π, and all three sub-components are occupied. The phase dynamics equation for all the sub-components is set to 0. Under the Thomas-Fermi approximation and setting the phase dynamics equations (eqn.2.4 - eqn.2.6) to 0 gives us

$$U_{trap}(r) - \mu + c_0 n - p + q - (\sqrt{n_{-1}} - \sqrt{n_1})\frac{c_1 n_0}{\sqrt{n_1}} = c_1(n_{-1} - n_1), \tag{2.43}$$

$$U_{trap}(r) - \mu + c_0 n + p + q - (\sqrt{n_1} - \sqrt{n_{-1}})\frac{c_1 n_0}{\sqrt{n_{-1}}} = -c_1(n_{-1} - n_1), \tag{2.44}$$

$$U_{trap}(r) + c_0 n + c_1(n_{-1} + n_1 - 2\sqrt{n_{-1} n_1}) - \mu = 0. \tag{2.45}$$

.

For APM state, $n_1(r) + n_{-1}(r) + n_0(r) = n(r)$.

Further, one can solve eqn.(2.35)-eqn.(2.37) to get the number density functions

$$n_1(r) = \frac{q^2+p^2+2pq}{4q^2}\left(n(r) - \frac{p^2-q^2}{2c_1 q}\right), \tag{2.46}$$

$$n_{-1}(r) = \frac{p^2+q^2-2pq}{4q^2}\left(n(r) - \frac{p^2-q^2}{2c_1 q}\right), \tag{2.47}$$

$$n_0(r) = \frac{(q^2-p^2)}{2q^2}\left(n(r) - \frac{q^2+p^2}{2c_1 q}\right), \tag{2.48}$$

and

$$n(r) = \frac{\mu + \frac{p^2-q^2}{2q} - U_{trap}(r)}{c_1+c_0}. \tag{2.49}$$

Finally, using the equations for sub-component number densities and total number density, one can find the expression for energy density

$$e_{APM}^{TF}(r) = U_{trap}(r)\left(\frac{k_2 - U_{trap}(r)}{c_1+c_0}\right) + \frac{c_0}{2}\left(\frac{k_2 - U_{trap}(r)}{c_1+c_0}\right)^2 + \frac{c_1}{2}\left(\frac{k_2 - U_{trap}(r)}{c_1+c_0} - \frac{p^2-q^2}{2qc_1}\right)^2, \tag{2.50}$$

where $k_2 = \mu + \frac{p^2-q^2}{2q}$.

2.2 Moving into nondimensional regime

Before introducing the actual Variational method, let's transform the existing equations into dimensionless form. We would consider that the Spin-1 BEC is confined in a quasi-one-dimensional harmonic potential elongated in the x-direction with a trapping frequency of ω_x. Furthermore, we would assume that the trapping frequency along y and z direction, i.e., ω_y and ω_z ($\omega_{y,z} >> \omega_x$). Oscillator length scale along the transverse direction is defined as $l_{yz} = \sqrt{\frac{\hbar}{m.\omega_{yz}}}$, where $\omega_{yz} = \sqrt{\omega_y \omega_z}$ and along the x-axis is defined as $l_x = \sqrt{\frac{\hbar}{m.\omega_x}}$.

To obtain the dimensionless phase equations for a BEC in a quasi 1d harmonic confinement, the scaling transformations for number densities and other parameters are as follows [16]

$$\frac{x}{l_x} = \zeta \quad , \quad p' = \frac{p}{\omega_x \hbar} \quad , \quad q' = \frac{q}{\omega_x \hbar} \quad , \quad \frac{\mu}{\omega_x \hbar} = \mu' \tag{2.51}$$

$$n_m .2\pi l_{yz}^2 l_x = u_m \tag{2.52}$$

$$\frac{c_0}{2\pi l_{yz}^2 l_x \hbar \omega_x} = \lambda_0 \qquad and \qquad \frac{c_1}{2\pi l_{yz}^2 l_x \hbar \omega_x} = \lambda_1 \tag{2.53}$$

where u_m is the number density for m^{th} sub-component in dimensionless form. q' and p' represent the nondimensional forms of quadratic and linear Zeeman terms, respectively. λ_0 and λ_1 represent the nondimensional forms for spin-independent and spin-dependent interaction coefficients, respectively. μ' denotes the chemical potential in dimensionless form.

Applying the scaling transformations (eqn.(2.51)-eqn.(2.53)) to sub-component evolution equation (eqn.(2.2), eqn.(2.3)), we would get

$$\dot{u_0}(\zeta) = -4\lambda_1 u_0 \sqrt{u_1 u_{-1}} \sin\theta_r, \tag{2.54}$$

$$\dot{u}_{\pm 1}(\zeta) = 2\lambda_1 u_0 \sqrt{u_1 u_{-1}} \sin\theta_r. \tag{2.55}$$

Applying the Scaling transformations, the phase stationary equation (eqn(2.4)- eqn(2.6) transforms into

$$\sqrt{u_0}\left(-\frac{1}{2}.\frac{d^2}{d\zeta^2} + \frac{\zeta^2}{2} - \mu' + \lambda_0 u + \lambda_1(u_{-1} + u_1 + 2\cos\theta_r \sqrt{u_{-1}u_1}\right) = 0, \tag{2.56}$$

$$\left(-\frac{1}{2}.\frac{d^2}{d\zeta^2}+\frac{\zeta^2}{2}+\lambda_0 u+q'-\lambda_1\left(u_{-1}-u_1\right)-\mu'-p'\right)\sqrt{u_1}+\lambda_1 u_0\left(\sqrt{u_1}+\sqrt{u_{-1}}\cos\theta_r\right)=0, \tag{2.57}$$

and

$$\left(-\frac{1}{2}.\frac{d^2}{d\zeta^2}+\frac{\zeta^2}{2}+\lambda_0 u+\lambda_1\left(u_{-1}-u_1\right)-\mu'+q'+p'\right)\sqrt{u_{-1}}+\left(\sqrt{u_1}\cos\theta_r+\sqrt{u_{-1}}\right)\lambda_1 u_0=0. \tag{2.58}$$

The same scaling transformations also transform the expression of energy density in eqn.(2.7) to

$$\begin{aligned} e(\zeta)=\Bigg[\sum_{m=-1}^{1}\left(-\sqrt{u_m(\zeta)}\frac{1}{2}\frac{d^2}{d\zeta^2}\sqrt{u_m(\zeta)}+\frac{\zeta^2}{2}u_m(\zeta)\right)+q'(u_{-1}+u_1)-p'(u_1-u_{-1}) \\ +\frac{\lambda_0}{2}u^2(\zeta)+\lambda_1\left(\frac{u_{-1}}{\sqrt{2}}-\frac{u_1}{\sqrt{2}}\right)^2+\lambda_1 u_0(u_1+2\cos\theta_r\sqrt{u_{-1}u_1}+u_{-1})\Bigg]. \end{aligned} \tag{2.59}$$

Furthermore, from here on, one can follow the same path in Section 2.1.1 and 2.1.2 and calculate the energy densities and number density expressions. We have summarized the energy densities and number density equations for individual stationary states in table 2.1

2.3 Previous Variational Method

There was a number density function that was founded by Arijit Bhattacharyay and Projjwal Kanti Kanjilal [15, 14], which they utilized to study the Polar-PM phase boundary. The number density function was as follows:

$$u(\zeta)=\begin{cases} g(\mu',\zeta), & \text{if } \zeta<\zeta_0 \\ (a+c\zeta+d\zeta^2)exp(-\frac{\zeta^2}{b}), & \text{if } \zeta\geq\zeta_0 \end{cases} \tag{2.60}$$

Where $g(\mu',\zeta)$ is the number density function for different stationary states under the Thomas-Fermi limit (as discussed in 2.1.1 and 2.1.2). Here, ζ_0 is the matching point that helps us to divide the number density function into two regions. The parameters a,b,c, and d are determined by ensuring smoothness and continuity at ζ_0. This is achieved by matching the number density, the first derivative of number density, and up to the third derivative for both regions at ζ_0. Furthermore, energy minimization concerning ζ_0 gives us the energy of a particular state. This minimization has fixed the value of ζ_0, giving the chemical potential (μ'). However, we later realized we could not use this number density function and method in the lower p regime to study the Anti

States	**number density variation**	**Energy density**
F1(1,0,0)	$u(\zeta)(\lambda_1+\lambda_0)=\mu'-q'+p'-\frac{\zeta^2}{2}$	$\frac{(\frac{\zeta^2}{2}-p'+q')(\mu'+p'-q'-\frac{\zeta^2}{2})}{\lambda_0+\lambda_1}+\frac{\left(\mu'+p'-q'-\frac{\zeta^2}{2}\right)^2}{2(\lambda_0+\lambda_1)}$
F2(0,0,1)	$u(\zeta)(\lambda_1+\lambda_0)=\mu'-\frac{\zeta^2}{2}-q'-p'$	$\frac{(\frac{\zeta^2}{2}+p'+q')(\mu'-p'-q'-\frac{\zeta^2}{2})}{\lambda_0+\lambda_1}+\frac{\left(\mu'-p'-q'-\frac{\zeta^2}{2}\right)^2}{2(\lambda_0+\lambda_1)}$
P(0,1,0)	$\lambda_0 u(\zeta)=\mu'-\frac{\zeta^2}{2}$	$\frac{\frac{\zeta^2}{2}(\mu'-\frac{\zeta^2}{2})}{\lambda_0}+\frac{\left(\mu'-\frac{\zeta^2}{2}\right)^2}{2\lambda_0}$
AF(1,0,1)	$\lambda_0 u(\zeta)=\mu'-q'-\frac{\zeta^2}{2}$ and $u_1-u_{-1}=\frac{p'}{\lambda_1}$	$\frac{(\frac{\zeta^2}{2}+q')(\mu'-q'-\frac{\zeta^2}{2})}{\lambda_0}+\frac{\left(\mu'-q'-\frac{\zeta^2}{2}\right)^2}{2\lambda_0}-\frac{p'^2}{2\lambda_1}$
PM(1,1,1)	$(\lambda_1+\lambda_0)u(\zeta)=k_2-\frac{\zeta^2}{2}$ where $k_2=\mu'+\frac{p'^2-q'^2}{2q'}$	$\frac{\zeta^2}{2}\left(\frac{k_2-\frac{\zeta^2}{2}}{\lambda_1+\lambda_0}\right)+\frac{\lambda_1}{2}\left(\frac{k_2-\frac{\zeta^2}{2}}{\lambda_1+\lambda_0}+\frac{q'^2-p'^2}{2q'\lambda_1}\right)^2$ + $\frac{\lambda_0}{2}\left(\frac{k_2-\frac{\zeta^2}{2}}{\lambda_1+\lambda_0}\right)^2$ and $\lvert p'\rvert<\lvert q'\rvert$
APM(1,1,1)	$(\lambda_1+\lambda_0)u(\zeta)=k_2-\frac{\zeta^2}{2}$ where $k_2=\mu'+\frac{p'^2-q'^2}{2q'}$	$\frac{\zeta^2}{2}\left(\frac{k_2-\frac{\zeta^2}{2}}{\lambda_1+\lambda_0}\right)+\frac{\lambda_1}{2}\left(\frac{k_2-\frac{\zeta^2}{2}}{\lambda_1+\lambda_0}+\frac{q'^2-p'^2}{2q'\lambda_1}\right)^2$ + $\frac{\lambda_0}{2}\left(\frac{k_2-\frac{\zeta^2}{2}}{\lambda_1+\lambda_0}\right)^2$ and $\lvert p'\rvert>\lvert q'\rvert$

Table 2.1: Energy densities and number density expressions for different stationary states of a spin-1 Bosonic Condensate under harmonic confinement in dimensionless form [16]

Ferromagnetic-Polar phase boundary.

Chapter 3

New Variational Method for determining the ground state Profile of a Spinor BEC under confinement

The previous chapter introduced the number and energy densities for all possible stationary states of Spinor Bosonic Condensates in the presence of a generic trapping potential, using the Thomas Fermi approximation. We also looked at a previously established Variational method that was used to find the phase boundary for trapped Spinor condensates. Furthermore, as we could not find the AF-Polar phase boundary with the previously established Variational method, there is a growing need for an analytic method to help us find any Phase boundary between stationary states. This chapter will examine a new Variational Method we designed to help us accurately estimate the number density function for a spin-1 condensate under harmonic confinement.

3.1 Determining a Number Density Function

In the next step, we used a single continuous function as our number density function. The variational wave function that we use for different sub-components is of the general form

$$\psi_m(\zeta) = (a_m - b_m\zeta^2)\exp\left(-\frac{\zeta^2}{2d_m}\right). \tag{3.1}$$

As we know, the number density function is given by $u_m = \psi_m\psi_m^*$, and since all our parameters are real, the number density function simplifies to $u_m = (\psi_m)^2$. Finally, the number density function

for individual sub-components becomes

$$u_m(\zeta) = \left[(a_m - b_m\zeta^2)\exp\left(-\frac{\zeta^2}{2d_m}\right)\right]^2. \tag{3.2}$$

Here u_m represents the density of m^{th} sub-component. a_m, b_m and d_m are parameters for different sub-components. The idea behind choosing this kind of function as our number density function is the following:

- Note that, for smaller values of ζ (i.e., close to the trap center), the interaction energy contribution (non-linear terms) is significant compared to the kinetic energy. Thus, we can omit the kinetic energy term (Thomas-Fermi approximations). Therefore, the individual sub-component number density functions or the total number density function of any stationary state should follow the structure of Thomas-Fermi approximated number densities (Table 2.1).

- Observe that, in the number density expression (eqn.3.2), the exponential term upon Taylor series expansion would generate terms of order ζ^2, ζ^4, and so on. Additionally, due to the presence of $(a - b\zeta^2)^2$ term, we can obtain a Thomas-Fermi structure for smaller values of ζ. On the contrary, choosing only $(a - b\zeta)^2$ would have resulted in terms involving ζ, ζ^2, which could not match the T-F profile for smaller values of ζ.

- At large values of ζ, our number density function should have a Gaussian profile in analogy with the ground state under harmonic oscillator potential.

3.2 Condensates having $\lambda_1 > 0$ under harmonic confinement

This section will introduce the Variational method for different stationary states that can serve as ground state candidates for a spin-1 BEC in a quasi 1d harmonic confinement with the anti-ferromagnetic type of spin interaction ($\lambda_1 > 0$ in dimensionless form or $c_1 > 0$ in actual dimensional form). From figure 1.1, we can observe that, for condensates having $c_1 > 0$, the Polar state, AF state, or one of the Ferromagnetic states (F1 and F2) act as the ground state depending on the values of quadratic and linear Zeeman terms.

3.2.1 Anti-Ferromagnetic or AF or (1,0,1) state

The AF state corresponds to the populated $m = -1, 1$ level and empty $m = 0$ level. For this multi-component state (AF), we will simplify our number density (eqn.3.2) by assuming the parameter

d_m for both sub-components to be equal, i.e., $d_1 = d_{-1} = d$. Thus, the sub-component number density and the total number density function become

$$\begin{aligned} u_1(\zeta) &= \left(a_1 - b_1\zeta^2\right)^2 \exp\left(-\frac{\zeta^2}{d}\right) \\ &= (a_1^2 + b_1^2\zeta^4 - 2a_1b_1\zeta^2)\exp\left(-\frac{\zeta^2}{d}\right), \end{aligned} \tag{3.3}$$

$$\begin{aligned} u_{-1}(\zeta) &= \left(a_{-1} - b_{-1}\zeta^2\right)^2 \exp\left(-\frac{\zeta^2}{d}\right) \\ &= (a_{-1}^2 + b_{-1}^2\zeta^4 - 2a_{-1}b_{-1}\zeta^2)\exp\left(-\frac{\zeta^2}{d}\right), \end{aligned} \tag{3.4}$$

and

$$\begin{aligned} u(\zeta) &= u_1(\zeta) + u_{-1}(\zeta) \\ &= \left[(a_1^2 + a_{-1}^2) + (b_1^2 + b_{-1}^2)\zeta^4 - (2a_1b_1 + 2a_{-1}b{-}1)\zeta^2\right]\exp\left(-\frac{\zeta^2}{d}\right). \end{aligned} \tag{3.5}$$

Observe that, we have 6 parameters, namely $a_1, a_{-1}, b_1, b_{-1}, d$ and chemical potential μ' (say).

Matching with Thomas-Fermi

We should note that, for smaller values of ζ (close to the trap center), the interaction energy contribution is significantly more significant than the kinetic energy. Thus, one can omit the kinetic energy (Thomas-Fermi approximation). So, in this regime, we can equate our number density function with the number density function calculated using the Thomas-Fermi approximation. However, the contributions from kinetic energy cannot be neglected for large values of ζ (i.e., far from the trap center).

Thus, for small values of ζ, the exponential term can be expanded using the Taylor Series, which would give us

$$exp(-\frac{\zeta^2}{d}) = 1 - \frac{\zeta^2}{d} + \frac{\zeta^4}{2d^2} + O(\zeta^6, \zeta^8, ..). \tag{3.6}$$

Using eqn.(3.6) in eqn.(3.5) and retaining only up to order 2 of ζ would give us the total number density

$$u(\zeta) = \left[(a_1^2 + a_{-1}^2) - \zeta^2\left(\frac{a_1^2}{d} + \frac{a_{-1}^2}{d} + 2a_1b_1 + 2a_{-1}b{-}1\right)\right]. \tag{3.7}$$

Our next step is to equate our number density function (eqn.(3.7)) with the T-F approximated number density function for small values of ζ. Here, we choose to equate our total number density function (eqn.(3.7)) to the total number density function calculated from the Thomas-Fermi

approximation (number density dimensionless equation of AF from table 2.1)

Equating the ζ^0 terms from both the equations gives us,

$$(a_1^2 + a_{-1}^2) = \frac{\mu' - q'}{\lambda_0} \tag{3.8}$$

The above equation fixes the chemical potential (μ') of the system by making it a function of a_1 and a_{-1},

$$\mu' = \lambda_0(a_1^2 + a_{-1}^2) + q' \tag{3.9}$$

Equating ζ^2 terms from both the equations will fix one of the parameters among a_1, a_{-1}, b_1, b_{-1} and d

$$\left(\frac{a_1^2}{d} + \frac{a_{-1}^2}{d} + 2a_1b_1 + 2a_{-1}b - 1\right) = \frac{1}{2\lambda_0} \tag{3.10}$$

Let us fix b_1 by making it a function of a_1, a_{-1}, b_{-1} and d as

$$b_1 = \frac{\left(\frac{1}{2\lambda_0} - \frac{a_1^2}{d} - \frac{a_{-1}^2}{d} - 2a_{-1}b - 1\right)}{2a_1}. \tag{3.11}$$

Finding other parameters

After we match our number density functions with the Thomas-Fermi, we are left with four parameters, namely a_1, a_{-1}, b_{-1} and d. Our next step is to minimize the free energy of our system concerning these parameters and use the number conservation equation as our constraint to get these parameters. Note that rather than simply minimizing the total energy to determine the parameters, we will employ the Lagrange multiplier method in the presence of a constraint. The following equations will fix the other parameters:

$$N - \left(\int n_{-1}(\zeta)\, d\zeta + \int n_1(\zeta)\, d\zeta\right) = 0, \tag{3.12}$$

$$\nabla_{a_1}\left(E - \mu'\left(\int n_{-1}(\zeta)\, d\zeta + \int n_1(\zeta)\, d\zeta\right)\right) = 0, \tag{3.13}$$

$$\nabla_{a_{-1}}\left(E - \mu'\left(\int n_{-1}(\zeta)\, d\zeta + \int n_1(\zeta)\, d\zeta\right)\right) = 0, \tag{3.14}$$

$$\nabla_{b_{-1}}\left(E - \mu'\left(\int n_{-1}(\zeta)\, d\zeta + \int n_1(\zeta)\, d\zeta\right)\right) = 0. \tag{3.15}$$

E represents the system's energy and is given by eqn.(1.14), and N denotes the total number of condensate particles. Our final step is to solve these four equations to get these four parameters

simultaneously fixed, and then we would have the energy of the system determined for a particular value of q', p', and N. A case study will be shown in the next chapter by comparing the number density functions obtained from our variational method with those obtained through numerical simulation [17].

3.2.2 Polar state

The polar state is marked by populated $m = 0$ and empty $m = 1, -1$ level. The number density function for $m = 0$ sub-component would be the same as the total number density function

$$\begin{aligned} u(\zeta) = u_0(\zeta) &= \left(a_0 - b_0\zeta^2\right)^2 \exp\left(-\frac{\zeta^2}{d_0}\right) \\ &= (a_0^2 + b_0^2\zeta^4 - 2a_0b_0\zeta^2)\exp\left(-\frac{\zeta^2}{d_0}\right). \end{aligned} \tag{3.16}$$

Here, we have four parameters, namely a_0, b_0, d_0 and μ'.

Matching with Thomas-Fermi

As discussed earlier, performing a Taylor series expansion of the exponential term (eqn. 3.6), substituting this expansion in eqn.(3.16), and retaining terms up to order 2 of ζ would give us,

$$u(\zeta) = \left[a_0^2 - \zeta^2\left(\frac{a_0^2}{d_0} + 2a_0b_0\right)\right] \tag{3.17}$$

Similarly, our next step is to equate our total number density function (eqn.3.17) with the T-F approximated total number density (number density dimensionless eqn. of polar from table 2.1) for smaller values of ζ.

Equating ζ^0 terms from both the equations will fix the chemical potential of the system by making it a function of only a_0,

$$a_0^2 = \frac{\mu'}{\lambda_0} \tag{3.18}$$

$$\mu' = \lambda_0 a_0^2 \tag{3.19}$$

Equating ζ^2 terms from both the equations will fix the parameter b_0

$$\left(\frac{a_0^2}{d_0} + 2a_0b_0\right) = \frac{1}{2\lambda_0} \tag{3.20}$$

$$b_0 = \frac{\left(\frac{1}{2\lambda_0} - \frac{a_0^2}{d_0}\right)}{2a_0} \tag{3.21}$$

Finding the parameters

After we match our number density functions with the Thomas-Fermi, we are left with two parameters, namely a_0 and d_0. Our next step is to minimize the free energy of our system concerning these parameters and use the number conservation equation as our constraint to get these parameters (as discussed, we would use the Lagrange multiplier method),

$$N - \left(\int n_0(\zeta)\, d\zeta\right) = 0, \tag{3.22}$$

$$\nabla_{a_0}\left(E - \mu' \int n_0(\zeta)\, d\zeta\right) = 0. \tag{3.23}$$

Here, E represents the local Energy density of the system and is given by eqn.(1.14), and N denotes the number of condensate particles. Finally, solving these two equations simultaneously will give us the remaining two parameters, and we will have our number density functions and total energy of the system for a particular value of N.

3.2.3 Ferromagnetic (F1) state

The F1 state is a single component state marked by empty $m = 0, -1$ level and populated $m = 1$. The number density function for $m = 1$ sub-component would be the same as the total number density function

$$\begin{aligned} u(\zeta) = u_1(\zeta) &= \left(a_1 - b_1\zeta^2\right)^2 \exp\left(-\frac{\zeta^2}{d_1}\right) \\ &= (a_1^2 + b_1^2\zeta^4 - 2a_1b_1\zeta^2)\exp\left(-\frac{\zeta^2}{d_1}\right). \end{aligned} \tag{3.24}$$

Here, we have four parameters, namely a_1, b_1, d_1 and μ'.

Matching with Thomas-Fermi

As discussed, doing a Taylor series expansion of the exponential term (eqn. (3.6)) and substituting it in eqn.(3.24) would give us,

$$u(\zeta) = \left[a_1^2 - \zeta^2\left(\frac{a_1^2}{d_1} + 2a_1b_1\right)\right]. \tag{3.25}$$

Our next step is to equate our total number density function(eqn. 3.33) with the T-F approximated total number density function (number density dimensionless eqn. of F1 state from table 2.1) for small values of ζ.

Equating ζ^0, ζ^2 terms from both the equations will fix μ' and b_1

$$a_1^2 = \frac{\mu' + p' - q'}{\lambda_0 + \lambda_1}, \tag{3.26}$$

$$\mu' = (\lambda_0 + \lambda_1)a_0^2 - p' + q', \tag{3.27}$$

and

$$\left(\frac{a_1^2}{d_1} + 2a_1 b_1\right) = \frac{1}{2(\lambda_0 + \lambda_1)}, \tag{3.28}$$

$$b_1 = \frac{\left(\frac{1}{2(\lambda_0+\lambda_1)} - \frac{a_1^2}{d_1}\right)}{2a_1}. \tag{3.29}$$

Finding the parameters

We are left with two parameters, namely a_1 and d_1. As discussed, using the Lagrange multiplier method with free energy minimization and a number constraint equation would help us get these parameters.

$$N - \left(\int n_1(\zeta)\, d\zeta\right) = 0 \tag{3.30}$$

$$\nabla_{a_1}\left(E - \mu' \int n_1(\zeta)\, d\zeta\right) = 0 \tag{3.31}$$

Finally, solving these two equations simultaneously would help us get the remaining two parameters, and we will have our number density functions along with the system's total energy for a particular value of q', p', and N.

3.2.4 Ferromagnetic (F2) state

The F2 state is a single component state marked by populated $m = -1$ and empty $m = 0, 1$ levels. The number density function for $m = -1$ sub-component would be the same as the total number density function

$$\begin{aligned} u(\zeta) = u_{-1}(\zeta) &= \left(a_{-1} - b_{-1}\zeta^2\right)^2 \exp\left(-\frac{\zeta^2}{d_{-1}}\right) \\ &= (a_{-1}^2 + b_{-1}^2\zeta^4 - 2a_{-1}b_{-1}\zeta^2)\exp\left(-\frac{\zeta^2}{d_{-1}}\right) \end{aligned} \tag{3.32}$$

Here, we have 4 parameters, namely a_{-1}, b_{-1}, d_{-1} and μ'.

Matching with Thomas-Fermi

As discussed, for smaller values of ζ, performing a Taylor series expansion of the exponential term (eqn. 3.6) and substituting it in eqn.(3.32) would give us

$$u(\zeta) = \left[a_{-1}^2 - \zeta^2 \left(\frac{a_{-1}^2}{d_{-1}} + 2a_{-1}b_{-1} \right) \right] \tag{3.33}$$

Furthermore, equating ζ^0 and ζ^2 terms from our total number density function(eqn. (3.33) With the total number density function calculated from T-F approximation(number density dimensionless eqn. of F2 state from table 2.1) for small values of ζ would give us,

$$a_{-1}^2 = \frac{\mu' - p' - q'}{\lambda_0 + \lambda_1}, \tag{3.34}$$

$$\mu' = (\lambda_0 + \lambda_1) a_{-1}^2 + p' + q', \tag{3.35}$$

and

$$\left(\frac{a_{-1}^2}{d_{-1}} + 2a_{-1}b_{-1} \right) = \frac{1}{2(\lambda_0 + \lambda_1)}, \tag{3.36}$$

$$b_{-1} = \frac{\left(\frac{1}{2(\lambda_0+\lambda_1)} - \frac{a_{-1}^2}{d_{-1}} \right)}{2a_{-1}}. \tag{3.37}$$

Finding the parameters

Using the Lagrange multiplier method discussed in the earlier sections, we can find the remaining two parameters, namely a_{-1} and d_{-1}.

$$N - \left(\int n_{-1}(\zeta)\, d\zeta \right) = 0 \tag{3.38}$$

$$\nabla_{a_{-1}} \left(E - \mu' \int n_{-1}(\zeta)\, d\zeta \right) = 0 \tag{3.39}$$

Solving these two equations simultaneously will give us the remaining two parameters, and we would have our number density functions along with the system's total energy for a particular value of q', p' and N.

3.3 Condensates with the absence of spin-spin interaction (Neutral condensate) under harmonic confinement

This section will introduce the variational method for different stationary states that can serve as ground state candidates for a spin-1 BEC in a quasi 1d harmonic confinement with no spin-spin interaction ($\lambda_1 = 0$ in dimensionless form or $c_1 = 0$ in actual dimensional form). From figure 1.1, we can observe that a condensate with the absence of spin-spin interaction (Neutral condensate) favors either the Polar state or one of the Ferromagnetic states (F1 and F2) as the ground state depending on the values of quadratic and linear Zeeman terms. In our previous section, we discussed the Variational method for the Polar state or any of the Ferromagnetic states (F1 or F2 state). However, one change compared to the last section is that while employing the variational method, we must substitute the value of λ_1 to be 0.

3.4 Condensates having $\lambda_1 < 0$ under harmonic confinement

This section will introduce the variational method for different stationary states that can serve as ground state candidates for a spin-1 BEC in a quasi 1-D harmonic trapping with the ferromagnetic type of spin interaction ($\lambda_1 < 0$ in dimensionless form or $c_1 < 0$ in actual dimensional form). From figure 1.1, we can observe that a condensate having $c_1 < 0$, Polar, (1,1,1) state (PM/APM state) or one of the Ferromagnetic states (F1 and F2) act as the ground state depending on the values of quadratic and linear Zeeman terms.

In the earlier section, we discussed the Variational method for the Polar state or any of the Ferromagnetic states (F1 or F2 state). However, compared to the earlier section, one change is that we must substitute a negative value of λ_1 while employing the variational method. From here onward, we will learn about using the Variational method for the Phase-matched (PM) state.

3.4.1 Phase-matched state(PM state)

The PM state is marked by all three sub-components ($m = 1, -1, 0$) being populated. For this multi-component state (PM), we would simplify our number density (eqn.3.2) by assuming the parameter d_m and b_m for all three sub-components to be equal i.e., $d_1 = d_{-1} = d_0 = d$ and $b_1 = b_{-1} = b_0 = b$. Thus, the number density function for different sub-components becomes

$$\begin{aligned} u_m(\zeta) &= \left(a_m - b\zeta^2\right)^2 \exp\left(-\frac{\zeta^2}{d}\right) \\ &= (a_m^2 + b^2\zeta^4 - 2a_m b\zeta^2) \exp\left(-\frac{\zeta^2}{d}\right), \end{aligned} \tag{3.40}$$

where m=1,-1,0 corresponds to different sub-components.

Our total number density function now becomes

$$\begin{aligned} u(\zeta) &= u_1(\zeta) + u_{-1}(\zeta) + u_0(\zeta) \\ &= \left[(a_1^2 + a_{-1}^2 + a_0^2) + 3b^2\zeta^4 - (2a_1b + 2a_{-1}b + 2a_0b)\zeta^2\right] \exp\left(-\frac{\zeta^2}{d}\right). \end{aligned} \tag{3.41}$$

We have 6 parameters, namely a_1, a_{-1}, a_0, b, d, and μ'.

Matching with Thomas-Fermi

As discussed, for smaller values of ζ, doing a Taylor series expansion of the exponential term (eqn.3.6) and substituting it in eqn.(3.41) would give us

$$u(\zeta) = \left[(a_1^2 + a_{-1}^2 + a_0^2) - \zeta^2\left(\frac{a_1^2}{d} + \frac{a_{-1}^2}{d} + \frac{a_0^2}{d} + 2a_1b + 2a_{-1}b + 2a_0b\right)\right] \tag{3.42}$$

Furthermore, equating the ζ^0 and ζ^2 terms from our total number density function (eqn. 3.42) with the T-F approximated total number density function(number density dimensionless equation of PM state from table 2.1) for small values of ζ would fix μ' and b, respectively,

$$(a_1^2 + a_{-1}^2 + a_0^2) = \frac{\mu' + \frac{(p')^2 - (q')^2}{2q'}}{\lambda_0 + \lambda_1}, \tag{3.43}$$

$$\mu' = (\lambda_0 + \lambda_1)(a_1^2 + a_{-1}^2 + a_0^2) - \left(\frac{(p')^2 - (q')^2}{2q'}\right), \tag{3.44}$$

and

$$\left(\frac{a_1^2}{d} + \frac{a_{-1}^2}{d} + \frac{a_0^2}{d} + 2a_1b + 2a_{-1}b + 2a_0b\right) = \frac{1}{2\lambda_1 + 2\lambda_0}, \tag{3.45}$$

$$b = \frac{\left(\frac{1}{2\lambda_1 + 2\lambda_0} - \frac{a_1^2}{d} - \frac{a_{-1}^2}{d} - \frac{a_0^2}{d}\right)}{2a_1 + 2a_0 + 2a_{-1}}. \tag{3.46}$$

Finding parameters

After we match the number density function with Thomas-Fermi, we are left with four parameters, namely a_1, a_{-1}, a_0, and d. As discussed, using the Lagrange multiplier method with free energy

minimization and number constraint equation will help us get these parameters

$$N - \left(\int n_{-1}(\zeta)\, d\zeta + \int n_1(\zeta)\, d\zeta + \int n_0(\zeta)\, d\zeta \right) = 0, \tag{3.47}$$

$$\nabla_{a_1} \left(E - \mu' \left(\int n_{-1}(\zeta)\, d\zeta + \int n_1(\zeta)\, d\zeta + \int n_0(\zeta)\, d\zeta \right) \right) = 0, \tag{3.48}$$

$$\nabla_{a_{-1}} \left(E - \mu' \left(\int n_{-1}(\zeta)\, d\zeta + \int n_1(\zeta)\, d\zeta + \int n_0(\zeta)\, d\zeta \right) \right) = 0, \tag{3.49}$$

$$\nabla_{a_0} \left(E - \mu' \left(\int n_{-1}(\zeta)\, d\zeta + \int n_1(\zeta)\, d\zeta + \int n_0(\zeta)\, d\zeta \right) \right) = 0. \tag{3.50}$$

Our final step is to solve these four equations simultaneously to get the remaining four parameters, and we would have our number density functions along with the system's total energy for a particular value of q', p', and N.

Chapter 4

Results and Discussion

The previous chapter discussed the variational method for different stationary states. This chapter will begin with a case study for the Antiferromagnetic state by comparing the number of density functions obtained from our variational method with those obtained through numerical simulation [17]. Then, we would determine the phase boundary between different stationary states for varying values of spin-dependent interaction coefficient.

4.1 Case Study for Antiferromagnetic (AF) state

As discussed, the AF state corresponds to empty $m = 0$ level and populated $m = 1, -1$ level. After understanding the Variational method(in section 3.2), we will consider a case study in this section. We are considering spin-1 ^{23}Na condensate(that possesses antiferromagnetic type of spin interaction) in a quasi 1-D, i.e., cigar-shaped harmonic trap. Oscillator lengths along the transverse direction $l_{yz} = 0.59\mu m$, while along the direction of elongation $l_x = 2.97\mu m$. The spin-dependent and spin-independent parameter values correspond to $\lambda_1 = 7.43 \times 10^{-4}$ and $\lambda_0 = 46.16 \times 10^{-3}$ respectively. We have also fixed the quadratic and linear Zeeman terms at $q' = -0.5$ and $p' = 0.2$, respectively, and the number of condensate particles N is taken to be 5000. AF state is energetically favorable for these parameter values as the ground state.

With these specific choices for $p', q', \lambda_0, \lambda_1$ and N,we find $a_1 = 24.9450$, $a_{-1} = 16.5228$, $b_1 = -0.56995$, $b_{-1} = -0.3709$, $d = 17.3755$ and $\mu' = 40.8252$. Therefore, our sub-component number densities can be expressed analytically as

$$u_1(\zeta) = \left(24.9450 + 0.56995\zeta^2\right)^2 \exp\left(-\frac{\zeta^2}{17.3755}\right), \tag{4.1}$$

$$u_{-1}(\zeta) = \left(16.5228 + 0.3709\zeta^2\right)^2 \exp\left(-\frac{\zeta^2}{17.3755}\right). \tag{4.2}$$

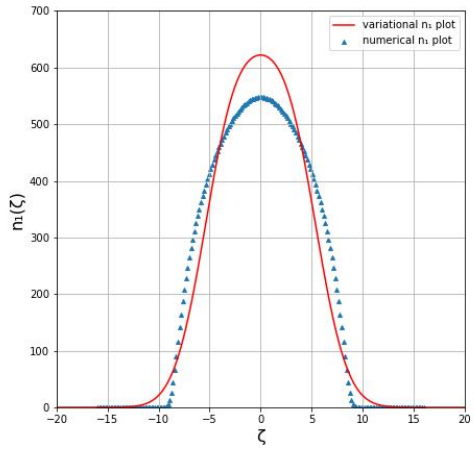

(a) Comparison of Variational method and numerical simulation [17] plots for n_1

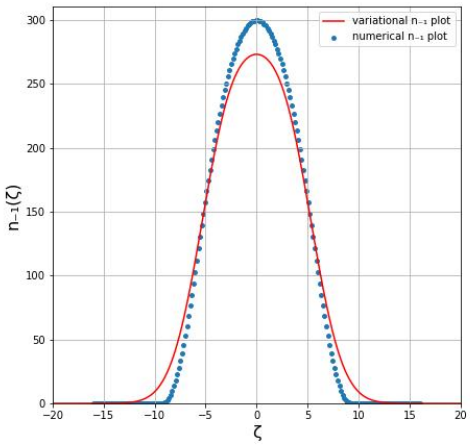

(b) Comparison of Variational method and numerical simulation [17] plots for n_{-1}

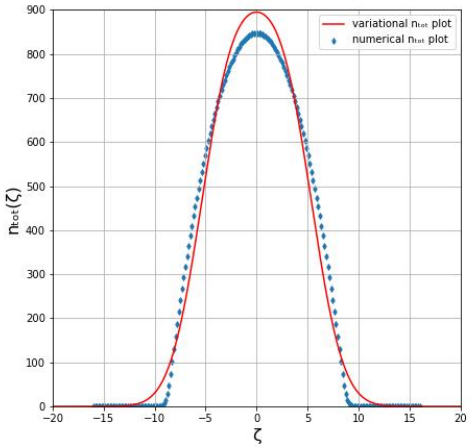

(c) Comparison of Variational method and numerical simulation [17] plots for n_{tot}

Figure 4.1: Comparison between Variational method and numerical simulation [17] plots

The results for number densities (u_1, u_{-1}, u_{total} in the dimensionless form or n_1, n_{-1}, n_{total} in dimensional form) are compared in the fig 4.1. We can see that the results of our variational method match quite well with numerical simulations [17] results.

4.2 Phase boundary for Condensates having $\lambda_1 > 0$ under harmonic confinement

In this part, we will use the variational method for a Spin-1 BEC in a quasi 1-D harmonic trapping with the antiferromagnetic type of spin interaction ($\lambda_1 > 0$ in dimensionless form or $c_1 > 0$ in actual dimensional form) and determine the phase boundary between different stationary states. We are considering spin-1 ^{23}Na condensate (which has $\lambda_1 > 0$) in a quasi 1-D harmonic potential. Oscillator lengths in the transverse direction $l_{yz} = 0.59\mu m$, while along the direction of elongation $l_x = 2.97\mu m$. The spin-independent parameter value corresponds to $\lambda_0 = 46.16 \times 10^{-3}$ and the spin-dependent parameter values corresponds to $\lambda_1 = 7.43 \times 10^{-4}$. We will begin by looking at the Polar-AF phase boundary and then map out the complete phase boundary for condensates having $c_1 > 0$.

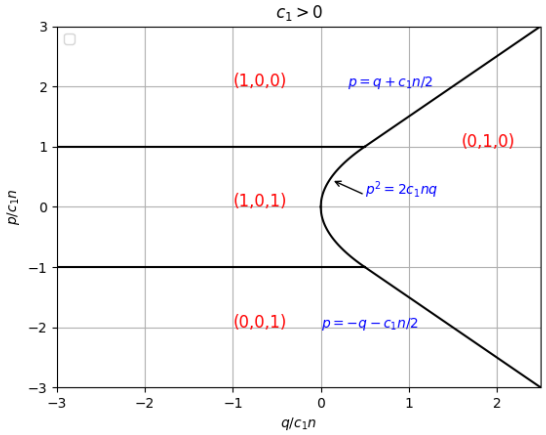

Figure 4.2: Homogenous phase boundary for $c_1 > 0$

The phase boundary for a homogeneous system with the antiferromagnetic type of spin interaction is shown in fig(4.2), which predicts the AF-Polar phase boundary to be Parabolic, Ferromagnetic-Polar phase boundary to be linear in nature and AF-Ferromagnetic phase boundary to be a constant curve.

4.2.1 Antiferromagnetic(AF)-Polar phase boundary

Using Section 3.2, we can estimate the total energy of the AF state for different values of q' and p'. We also learned how to find the total energy of the polar state using the variational method. Furthermore, we can compare the energies between the two competing states, which would reveal the phase boundary.

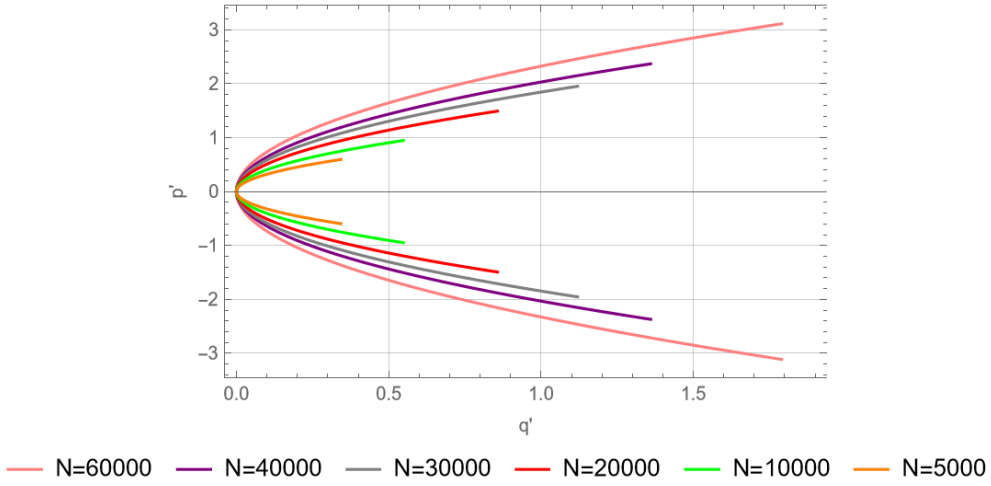

Figure 4.3: AF-polar phase boundary for a spin-1 condensate in a quasi 1-D harmonic confinement for different values of N

These plots (in the figure 4.3) fit well to the parabola equation of $p'^2 = Aq'$ (where A is the coefficient of Parabola). Furthermore, it would be interesting to see whether a scaling factor exists for trapped condensates that can collapse the phase boundaries for varying values of N to the same plot. The dependency of scaling factor A on N is determined by plotting $\log A$ vs $\log N$ for all N values (fig4.4).

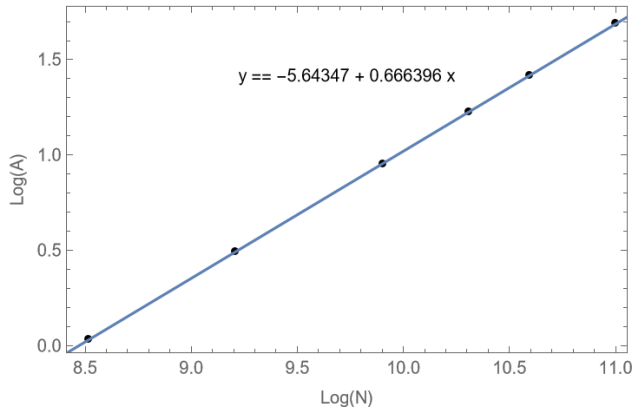

Figure 4.4: Variation of scaling factor A with number of condensate particles N

Assuming a power law dependence (i.e., $A \propto N^m$), we find from the fig 4.4 that the scaling

factor depends on N as $A \propto N^{2/3}$ ($0.6663 \approx \frac{2}{3}$) Next, looking at the AF-Polar phase boundary for different values of λ_1 would be interesting.

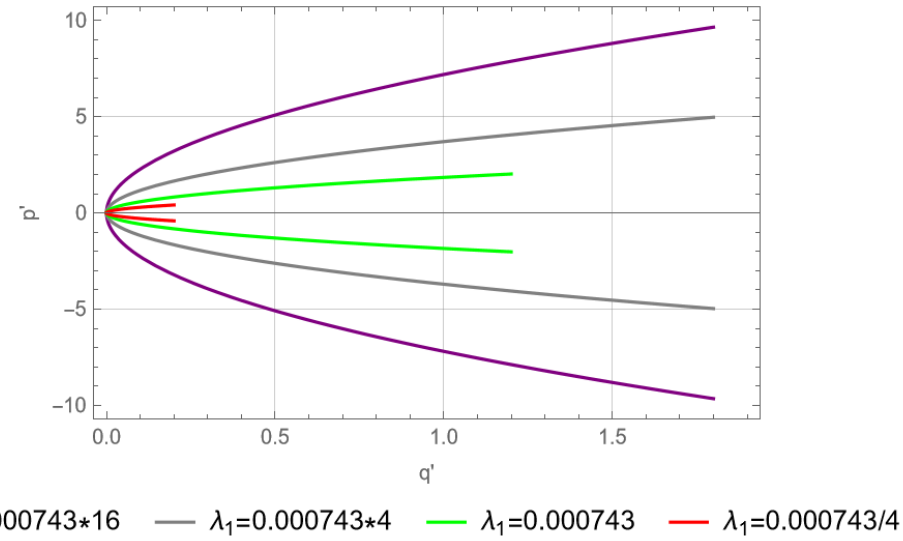

Figure 4.5: AF-polar phase boundary for different values of λ_1 with N=30000

The phase boundary in figure 4.5 is drawn by keeping N fixed at 30000 and varying the values of λ_1. Our next step will be to find a scaling factor that can bring all the phase boundaries for different values of λ_1 to the same plot.

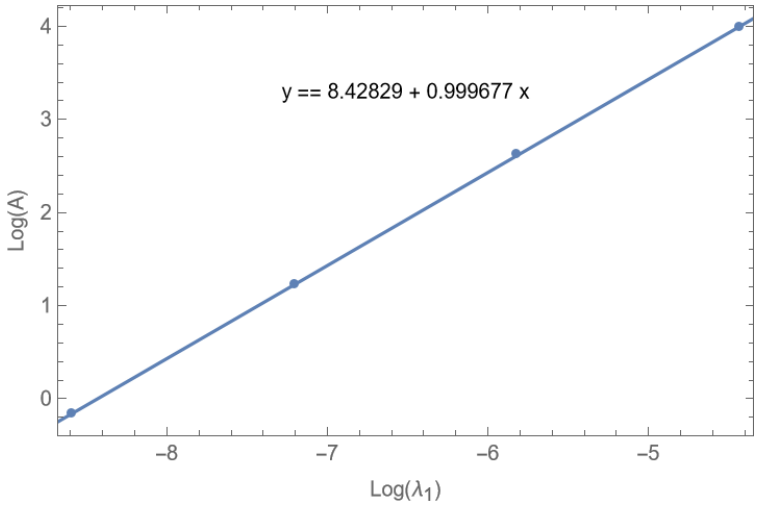

Figure 4.6: Variation of scaling factor A with λ_1

The dependence of scaling factor A upon the spin-dependent interaction coefficient(λ_1) is obtained by plotting $\log A$ vs $\log \lambda_1$ for all values of λ_1. Assuming a power law dependence (i.e.,

$A \propto \lambda^n$), we find from the figure 4.6 that the scaling factor depends on the spin-dependent parameter values roughly as $A \propto \lambda_1^1$.

Finally, through our variational method, we can find the universal AF-Polar phase boundary for a spin-1 BEC in a quasi 1d harmonic confinement, where the scaling factor $A \propto N^{2/3}\lambda_1^1$.

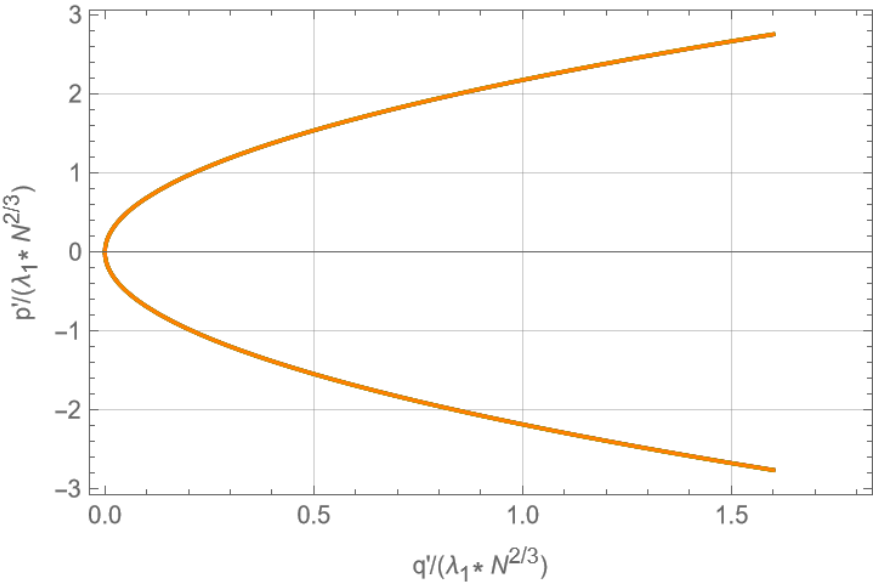

Figure 4.7: Universal AF-Polar phase boundary for Spin-1 Bosonic Condensate in a 1-D harmonic trap

As predicted by the homogeneous result, the parabolic nature of the AF-Polar phase boundary remains even in the case of Spin-1 Condensate in a quasi 1-D harmonic confinement.

4.2.2 Ferromagnetic(F1)-Polar phase boundary

As discussed, we can use the sec (3.2) to estimate the total energy of the Ferromagnetic (F1) state and Polar state. Furthermore, we can compare the energies between the two competing states, which would reveal the phase boundary.

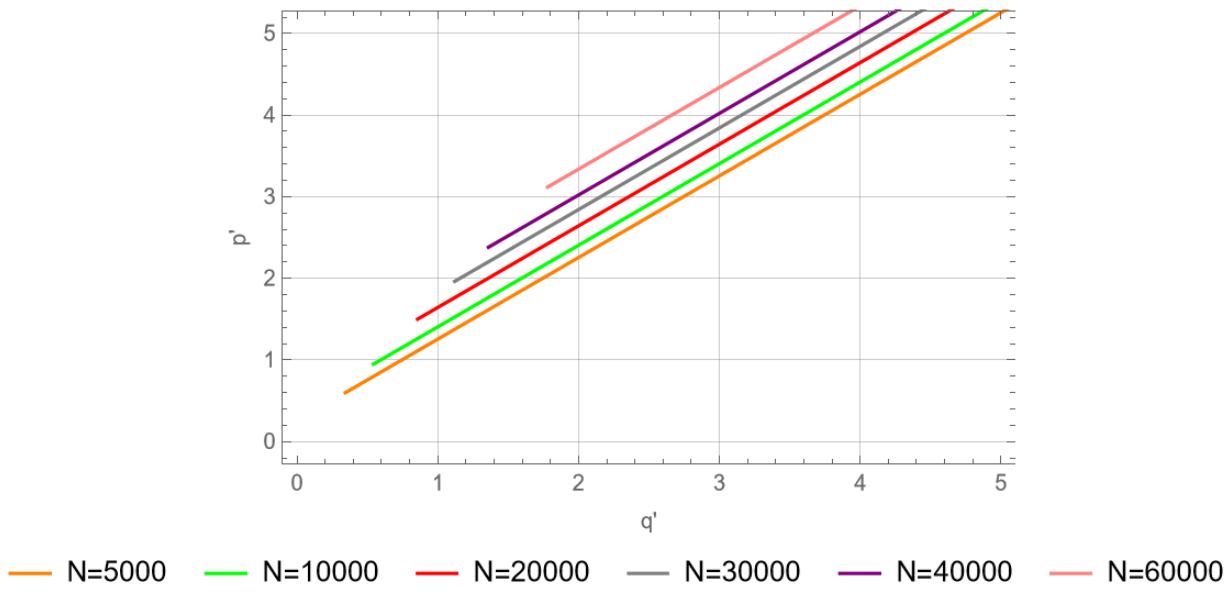

Figure 4.8: Ferromagnetic(F1)-polar phase boundary for different N values for a trapped spin-1 condensate

These plots (figure 4.8) fit well to a linear model i.e., $p' = q' + B$, where B is the coefficient that varies with N.

From here onward, we would follow the same path we followed to find the AF-polar phase boundary, i.e., we would check what kind of dependence B has on N and λ_1, and finally proceed to find the universal F1-polar phase boundary.

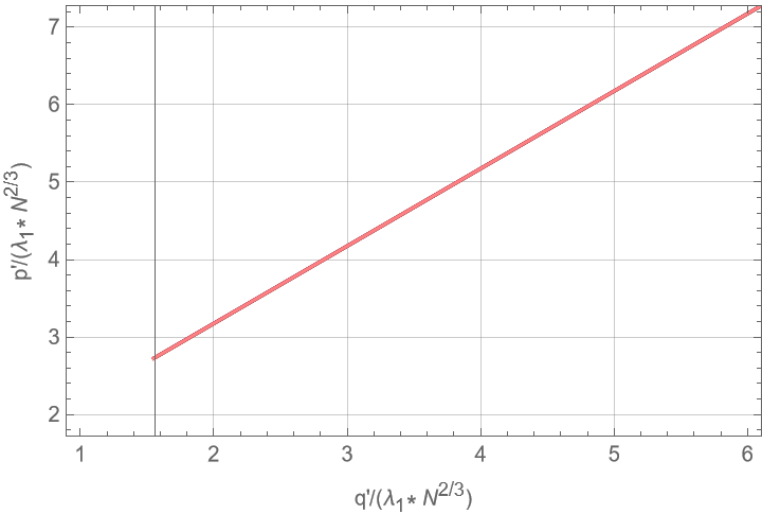

Figure 4.9: universal Ferromagnetic(F1)-Polar phase boundary

From the figure 4.9, one can see that the dependence of B on several condensate particles and

spin-dependent interaction coefficient is $B \propto N^{2/3}\lambda_1^1$. Similarly, we can draw the F2-Polar phase boundary as it would be symmetrical to the F1-Polar phase boundary about the x-axis.

Note that the linear nature of the Ferromagnetic-Polar phase boundary as predicted by the Homogenous result persists in harmonically trapped case.
It would also be interesting to look at the AF-polar, F1-polar, and F2-polar phase boundary for different N values and the universal phase boundary.

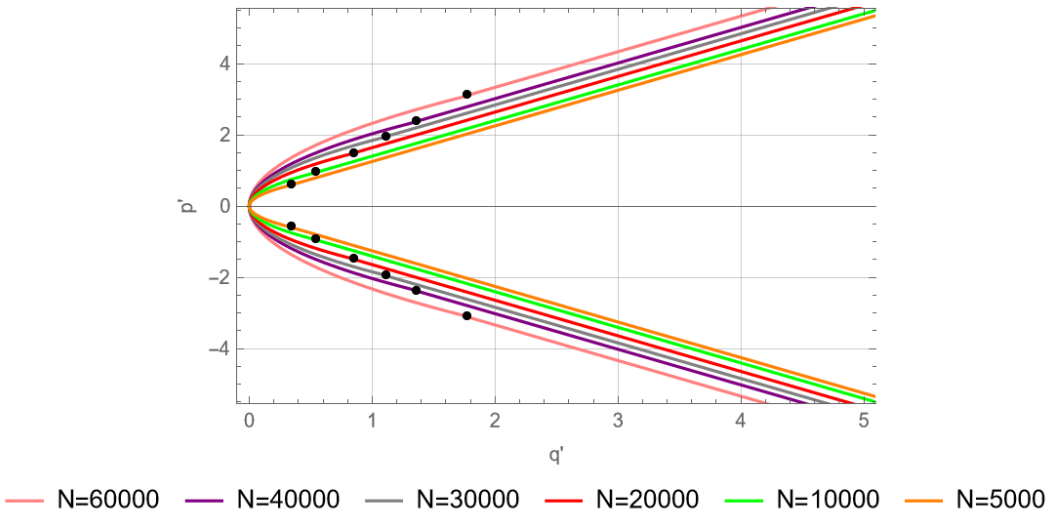

Figure 4.10: AF-Polar,F1-Polar and F2-Polar phase boundary for different values of N

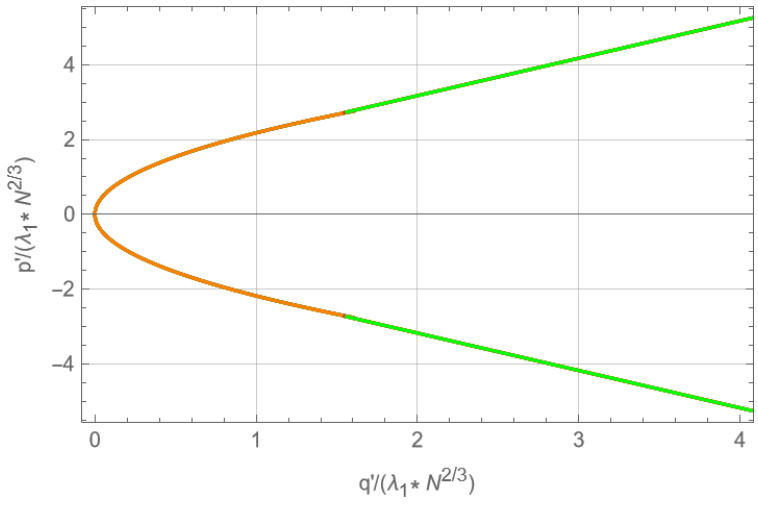

Figure 4.11: Universal AF-Polar,F1-Polar and F2-Polar phase boundary

4.2.3 Antiferromagnetic-Ferromagnetic (F1) phase boundary

Using sec (3.2), we can estimate the total energy of the Antiferromagnetic (AF) and Ferromagnetic(F1) state for different values of q' and p'. Furthermore, we can compare the energy of the two competing states, which would reveal the phase boundary.

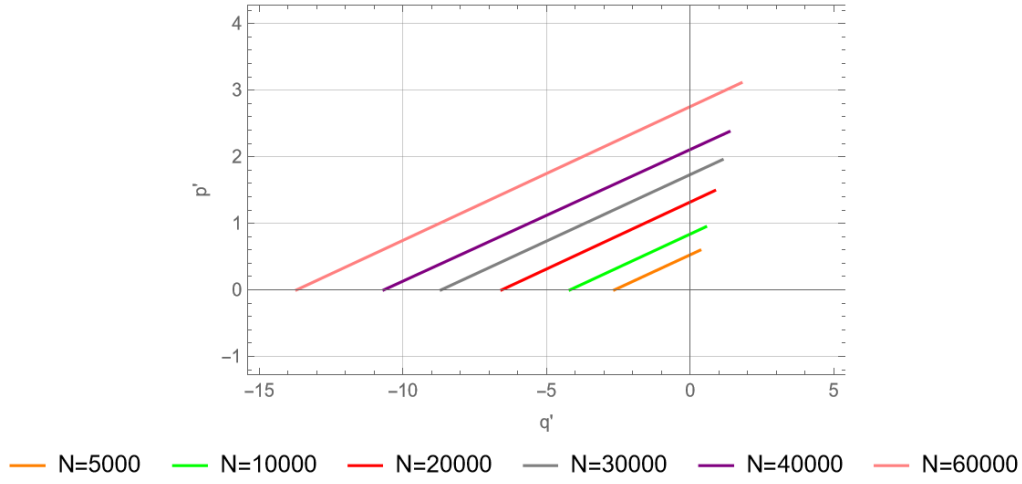

Figure 4.12: Anti-ferromagnetic(AF)-Ferromagnetic(F1) phase boundary for different N values

These plots (in the fig 4.12) fit well to linear fit, i.e., $p' = 0.2q' + C$ (where C is the coefficient that varies with N). From here onward, we would follow the same path we followed to find the phase boundary in the previous sections, i.e., we would check what kind of dependence C has on N and λ_1, then proceed to find the universal AF-F1 phase boundary.

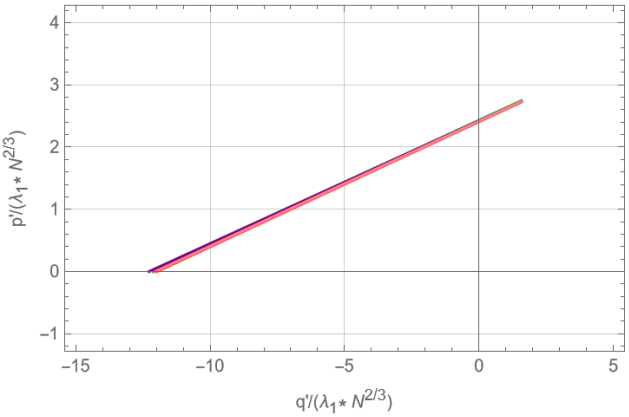

Figure 4.13: Universal Anti-ferromagnetic(AF)-Ferromagnetic(F1) phase boundary

From the figure (4.13), we can see that the dependence of C on several condensate particles and spin-dependent interaction coefficient is $C \propto N^{2/3}\lambda_1^1$. Similarly, we can also draw the AF-F2 phase boundary as it would be symmetrical to the AF-F1 phase boundary about the x-axis.

An interesting observation to note here is that the Anti Ferromagnetic - Ferromagnetic phase boundary for a Spin-1 BEC in a quasi 1-D harmonic confinement is a linear curve, which is different from what was predicted by the Homogenous result (Homogenous results as shown in figure 4.2 predicts the AF-Ferromagnetic phase boundary to be a constant line).

Finally, we have achieved the complete phase boundary for the case of Spin-1 Bose-Einstein Condensate with $\lambda_1 > 0$ (or $c_1 > 0$) in a quasi 1d harmonic trap for different values of N, and we have also obtained the complete universal phase boundary.

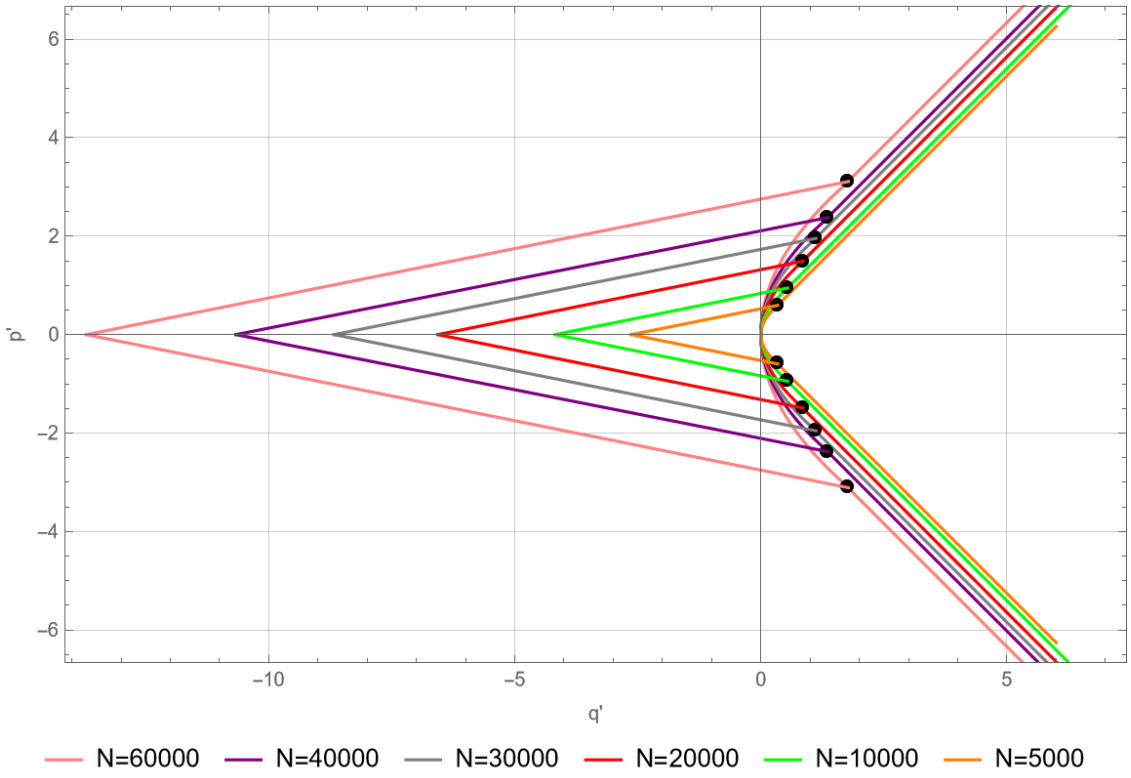

Figure 4.14: Complete phase boundary with $c_1 > 0$ or $\lambda_1 > 0$ for trapped condensates with varying values of N in (q', p') parameter space

An important observation to note by looking at the AF-Ferromagnetic phase boundary is that the AF state ceases to act as the ground state beyond a particular value of (q', p'), which forces us to calculate the F1-F2 phase boundary. The F1-F2 phase boundary, as observed through our Variational method, is a $p' = 0$ curve, which remains the same irrespective of the values of N.

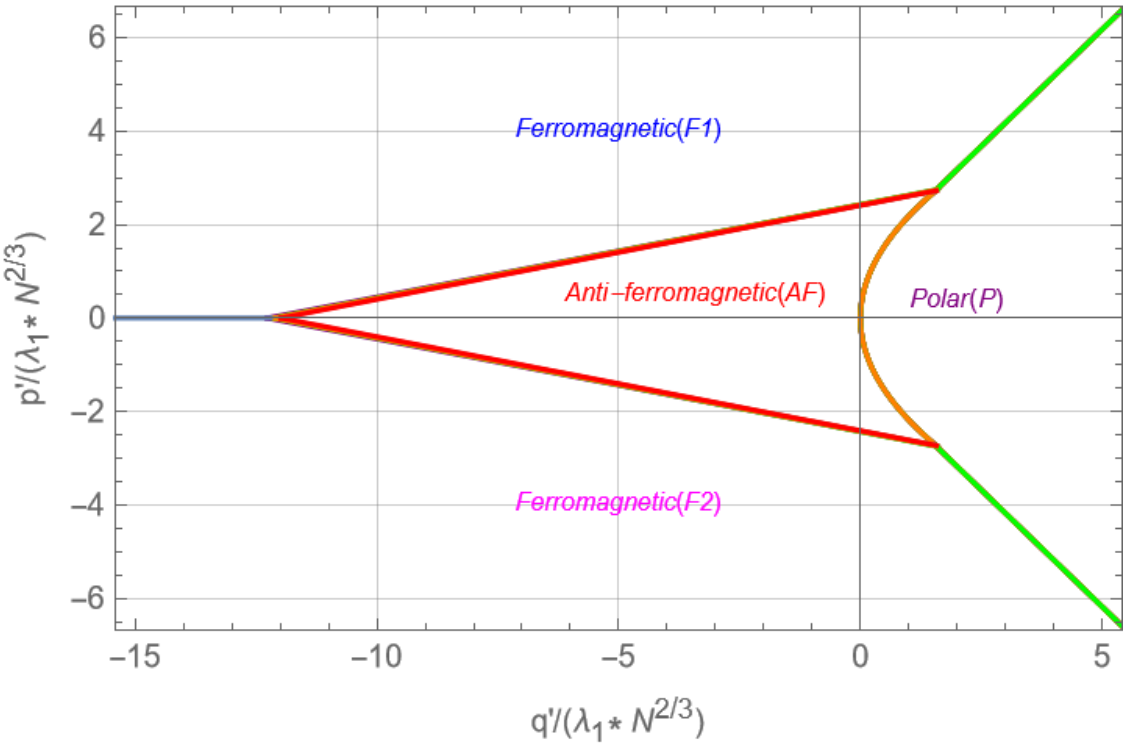

Figure 4.15: Universal phase boundary for Spin-1 Condensate with $\lambda_1 > 0$ in a quasi 1-D harmonic trap

We can see from figure 4.15 that, contrary to homogeneous results, if $\frac{q'}{\lambda_1 N^{2/3}} < -12$ (approx), the Antiferromagnetic state will not act as the ground state for a trapped Spin-1 Bosonic Condensate (with $\lambda_1 > 0$).

4.3 Phase boundary for condensates in absence of spin spin interaction(Neutral Condensates) under harmonic confinement

In this part, we will use the Variational method for a Spin-1 condensate under quasi 1d harmonic confinement with no spin-dependent interactions ($\lambda_1 = 0$ in dimensionless form or $c_1 = 0$ in actual dimensional form) and estimate the phase boundary between the competing ground states. Additionally, the spin-independent parameter corresponds to $\lambda_0 = 46.16 \times 10^{-3}$.We can refer to section (3.3) regarding the Variational method for F1, F2, and polar state. Furthermore, an energy comparison between the competing ground states would reveal the phase boundary. The phase boundary (shown in figure 4.16) remains constant irrespective of different N values and matches precisely to the phase boundary as predicted by homogeneous results (see fig 1.1)

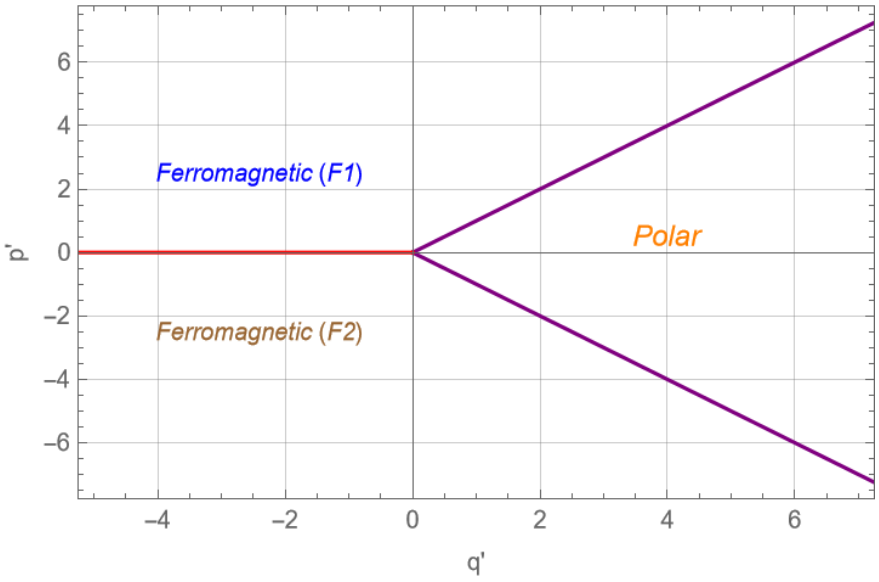

Figure 4.16: Universal phase boundary for Condensates with no spin-spin interaction($\lambda_1 = 0$) in a quasi 1-D harmonic confinement

4.4 Phase boundary for Condensates having $\lambda_1 < 0$ under harmonic confinement

In this part, we will use the variational method for a Spin-1 BEC in a quasi 1-D harmonic trapping having $\lambda_1 < 0$ (or $c_1 < 0$) and determine the phase boundary between different stationary states. We are considering spin-1 ^{87}Rb condensate (which has $\lambda_1 < 0$) in a quasi 1-D harmonic confinement. Oscillator lengths in the transverse direction $l_{yz} = 0.30\mu m$, while along the direction of elongation $l_x = 1.53\mu m$. The spin-independent parameter value corresponds to $\lambda_0 = 17.66 \times 10^{-2}$, and the spin-dependent parameter value corresponds to $\lambda_1 = -6.22 \times 10^{-4}$. We will begin by looking at the Polar-PM phase boundary and then map out the complete boundary.

The phase boundary for a homogeneous system with $c_1 < 0$ is shown in fig(1.1), which predicts the Polar-PM phase boundary to be hyperbolic, Ferromagnetic-PM phase boundary to be linear and the phase boundary between the two ferromagnetic states to be a constant curve with p=0.

4.4.1 Polar-PM phase boundary

Using Section 3.4, we can estimate the Polar state's and PM state's total energy. Furthermore, we can compare energy levels between the two competing states, which would reveal the phase boundary.

These plots (in the figure 4.17) fit well to the hyperbola equation of $p'^2 = 6.48q'^2 - B$(where B is the term that varies with N). As the term B has an N dependence, finding the depen-

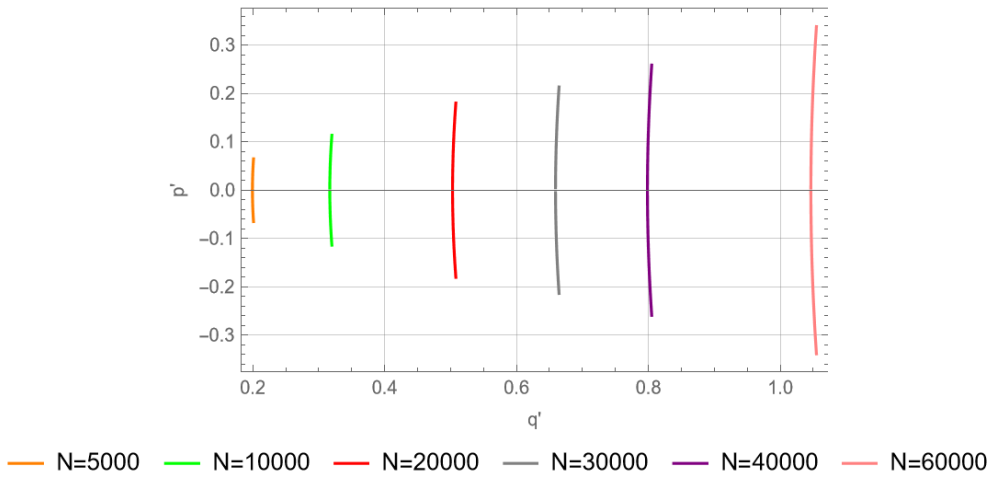

Figure 4.17: Polar-PM phase boundary for a spin-1 condensate in a quasi 1-D harmonic confinement for different values of N

dence(assuming a power law dependence, i.e., $B \propto N^k$) and subsequently finding the universal Polar-PM phase boundary would be fascinating.

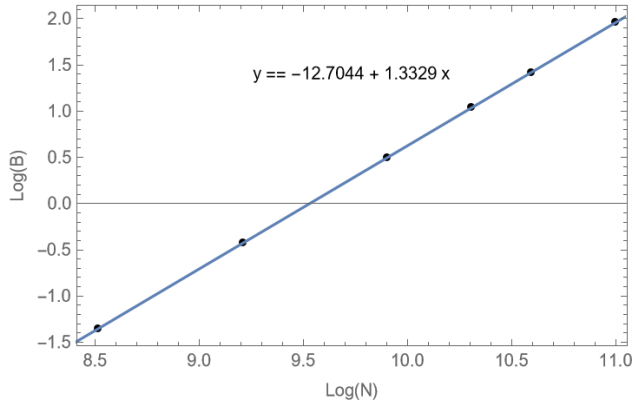

Figure 4.18: Variation of scaling factor B with N

From figure 4.18, we can interpret that $B \propto N^{1.3329}$.Subsequently, the scaling factor becomes $N^{0.66649}$. With this scaling factor, our Polar-PM boundary collapse is shown in figure 4.19.

With this scaling factor, we can observe that the collapse of the Polar-PM phase boundary for different N values is not perfect. This situation demands an improvement to our previously found scaling factor, i.e., $k_{new} = 0.66649 + \delta$. Interestingly, fixing δ around 0.0003 improves the universal Polar-PM phase boundary (Fig.4.20).

As predicted by the homogeneous results, the hyperbolic nature of the Polar-PM phase boundary persists for trapped condensates.

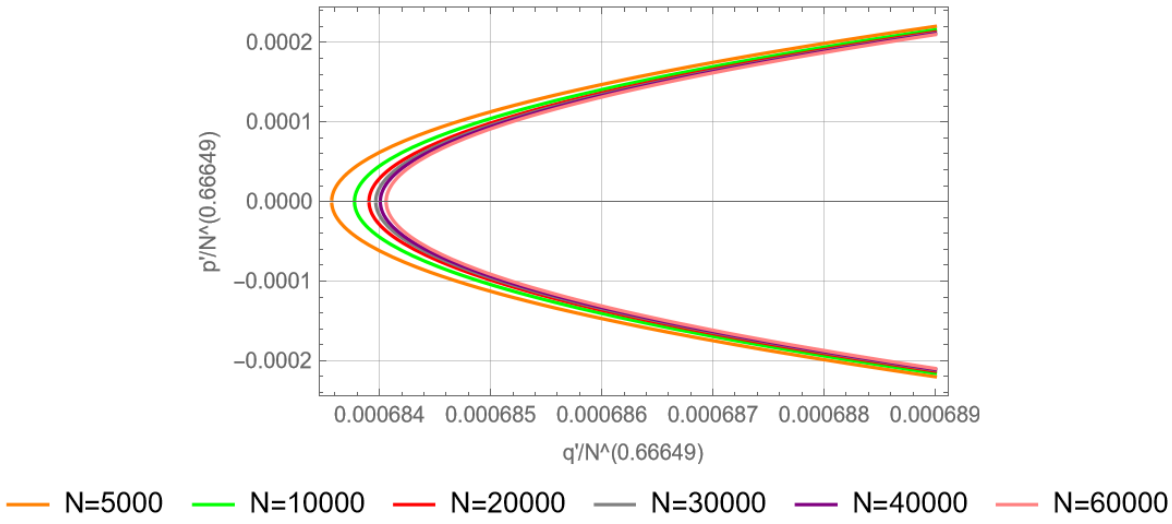

Figure 4.19: Universal Polar-PM phase boundary with scaling of 0.66649

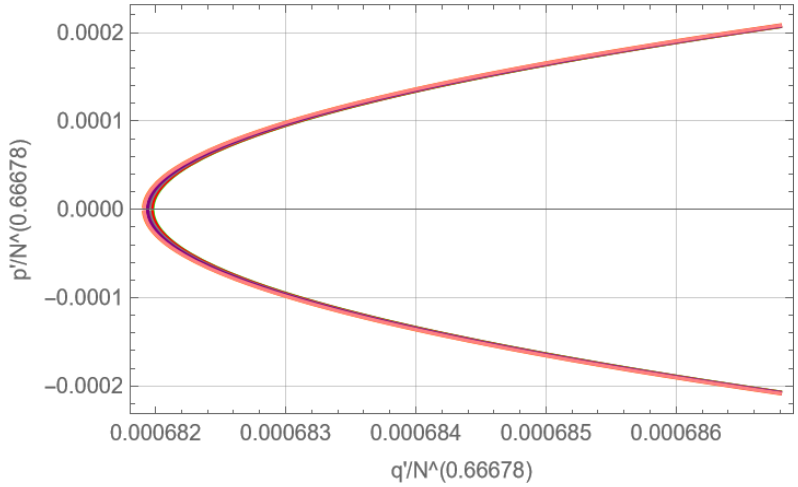

Figure 4.20: Universal Polar-PM phase boundary with scaling of 0.66678

4.4.2 Ferromagnetic-PM phase boundary

Using the Variational method, we can find the energies of both Ferromagnetic and PM states, and a comparison of energy between the two would reveal the phase boundary. These plots (fig 4.21) fit well to the linear fit, i.e., $p' = 0.38q' - C$ (where C has an N dependence). From here onward, we will find the N dependency in C and proceed to find the universal Ferromagnetic-PM phase boundary.

Note that the Ferromagnetic-PM phase boundary is a linear curve with a different functional form than the homogeneous predictions (which predicts the Ferromagnetic-PM phase boundary to be $p = q$ curve). An important observation is that the polar-PM and ferromagnetic-PM phase boundaries will intersect at a particular value of (q', p'). Beyond this intersection point, we have

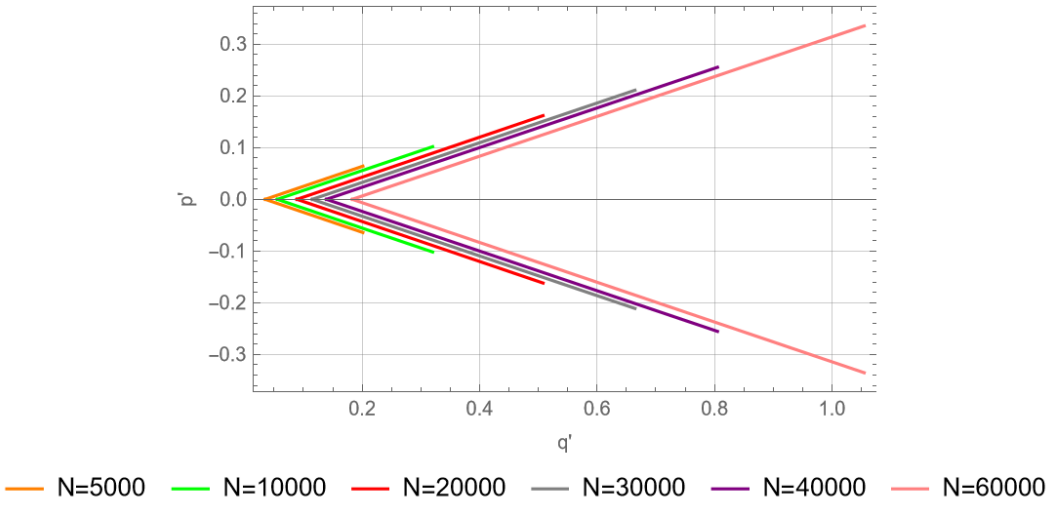

Figure 4.21: Ferromagnetic-PM phase boundary for different values of N

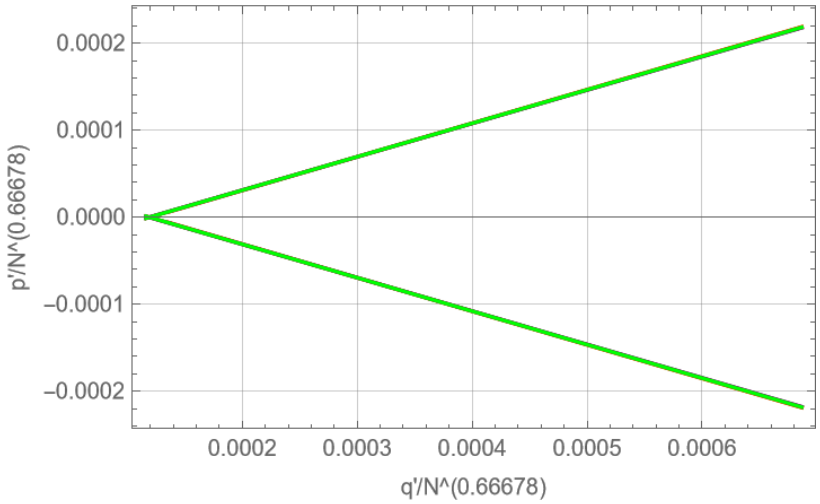

Figure 4.22: Universal Ferromagnetic-PM phase boundary for trapped condensates

to calculate the Polar-Ferromagnetic phase boundary, which was missing from the homogeneous results.

4.4.3 Polar-Ferromagnetic phase boundary

Following the path we followed in our previous sub-sections, we can find the Ferromagnetic-Polar phase boundary for different N values and the universal phase boundary. These plots (figure 4.23) fit well to the linear fit, i.e., $p' = q' - D$ (where D has a N dependence). It would be interesting to look at the complete phase boundary for different N values and the universal phase boundary for $c_1 < 0$. Furthermore, the F1-F2 phase boundary is a constant curve with $p' = 0$.

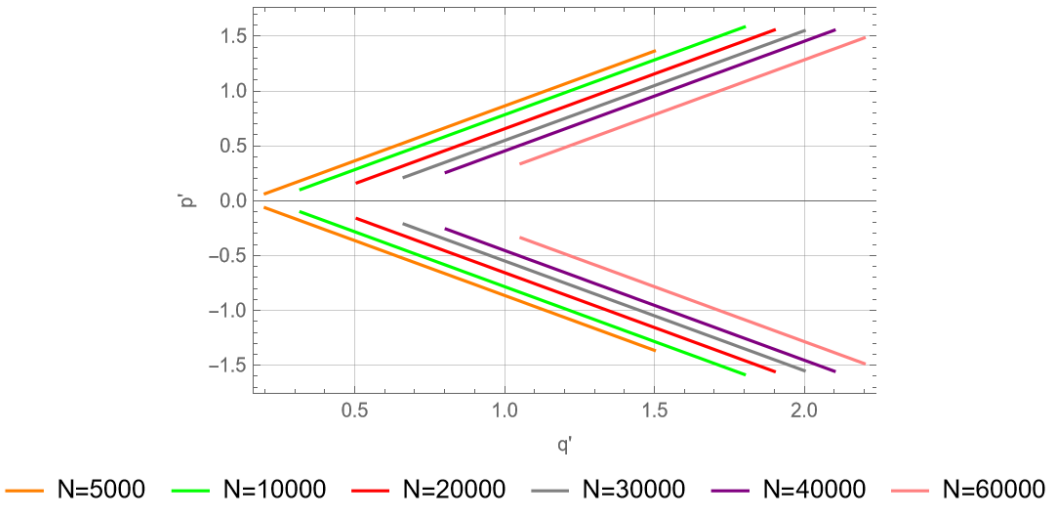

Figure 4.23: Ferromagnetic-Polar phase boundary for different values of N

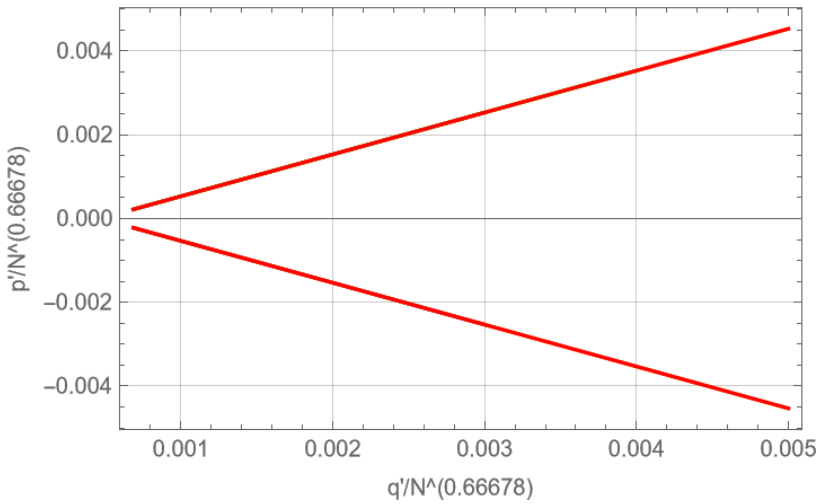

Figure 4.24: Universal Ferromagnetic-Polar phase boundary for trapped condensates

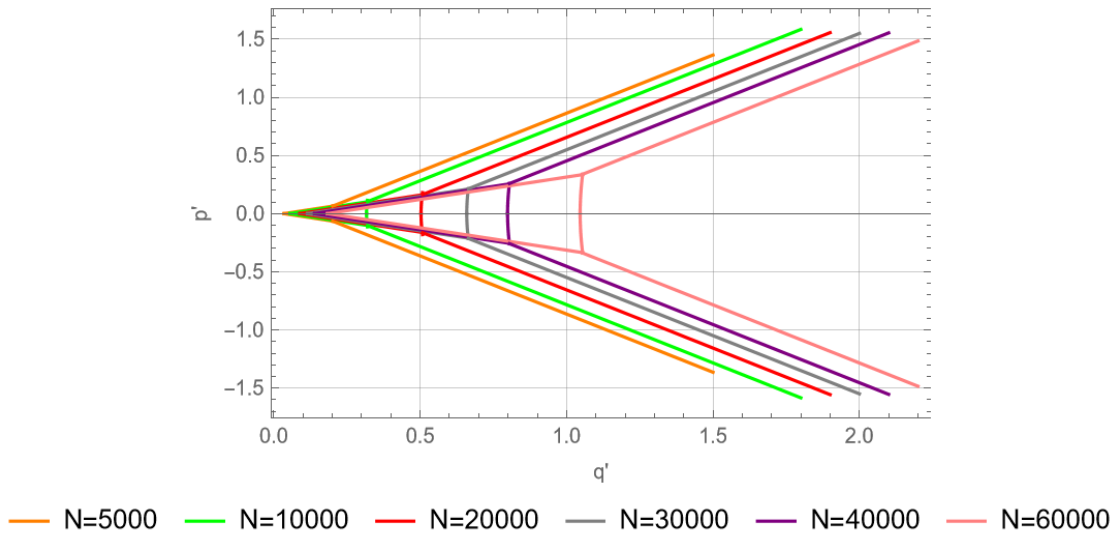

Figure 4.25: Complete phase boundary with $c_1 < 0$ or $\lambda_1 < 0$ for trapped condensates with varying values of N

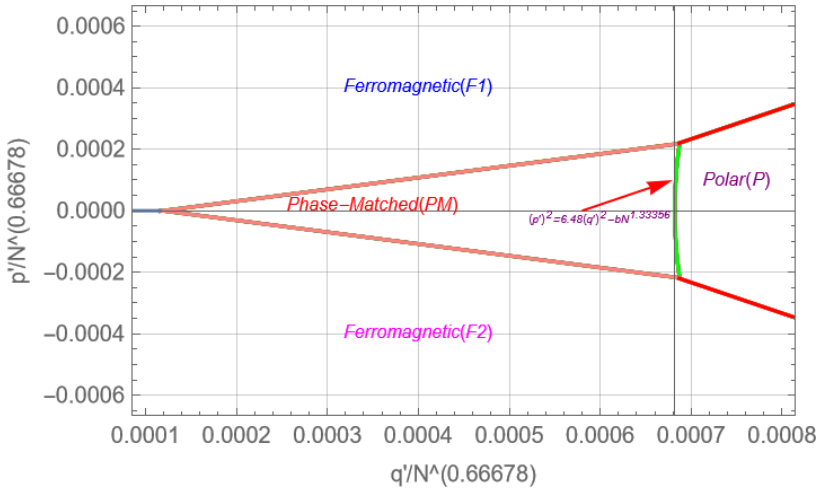

Figure 4.26: Universal phase boundary for trapped condensates with $c_1 < 0$ or $\lambda_1 < 0$

The universal Polar-PM phase boundary(green curve in the fig.4.26) is hyperbolic, with functional form of $p'^2 = 6.48q'^2 - bN^{1.33356}$($b$ is a constant of the order of 10^{-6}).

4.5 Comparison between homogeneous results and trapped systems

This section will compare the homogeneous results and trapped condensate results

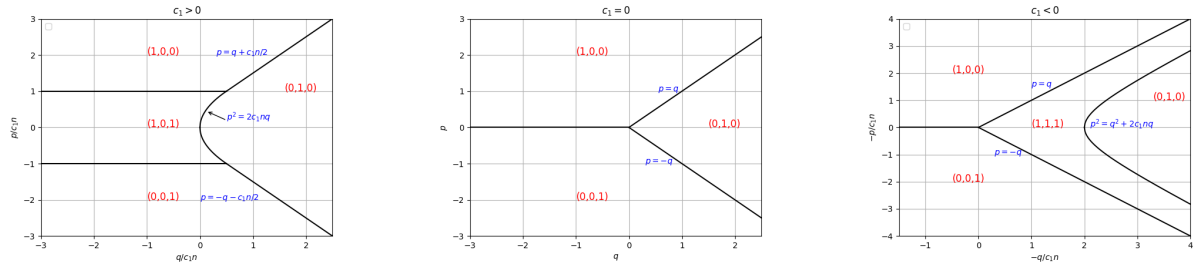

(a) $c_1 > 0$ (b) $c_1 = 0$ (c) $c_1 < 0$

Figure 4.27: phase diagram for spin-1 condensate in the absence of any trapping potential

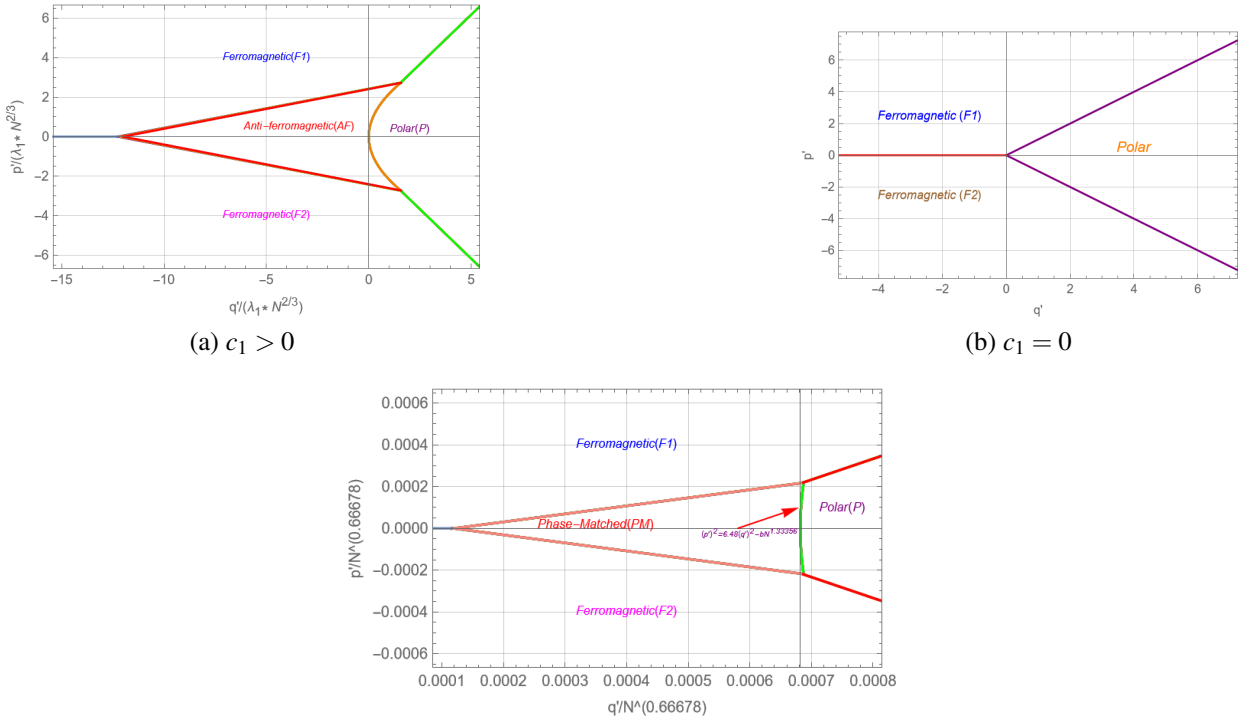

(a) $c_1 > 0$ (b) $c_1 = 0$

(c) $c_1 < 0$

Figure 4.28: Phase diagram for trapped spin-1 condensates

4.6 Energy density plots

In this section, we will use our Variational method to estimate the energy density plots as a function of distance from the trap center(ζ) for condensates with different types of spin interaction.(Note that we will show the energy density plots only for $\zeta > 0$; however,they would be symmetrical for $\zeta < 0$)

4.6.1 Energy density plot for condensate having $\lambda_1 > 0$

In this part, we will look at the energy density plots for the ground state candidates (F1, F2, AF, and Polar) of a spinor BEC in a harmonic confinement having $\lambda_1 > 0$. Our system is already described in Section 4.2. Additionally, we fix $p' = 0.15$, $q' = 0.2$ and $N = 5000$.

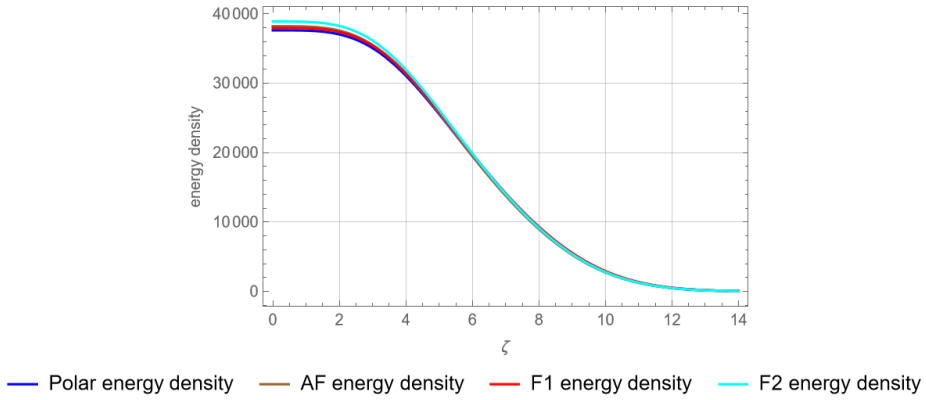

(a) energy density plots for different stationary states in a condensate(having $\lambda_1 > 0$), plotted against ζ, where $\zeta = 0$ is the 1-D trap center

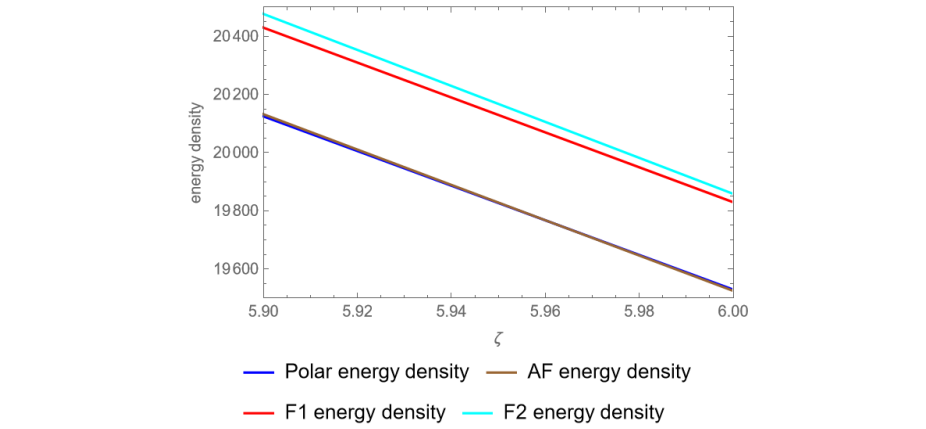

(b) energy density plots between $\zeta = 5.9$ to $\zeta = 6$, to show the crossing of energy density plots between different stationary states

Figure 4.29: Energy density plots for $\lambda_1 > 0$

4.6.2 Energy density plot for condensate having $\lambda_1 = 0$

In this part, we will look at the energy density plots for the ground state candidates (F1, F2, and Polar) of a spinor BEC in a harmonic confinement having $\lambda_1 = 0$. Our system is already described in Section 4.3. Additionally, we fix $p' = 0.4$, $q' = 0.5$ and $N = 5000$.

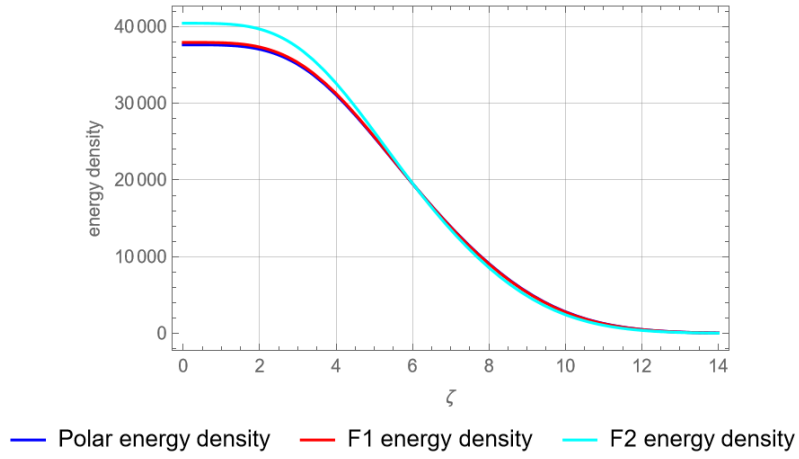

Figure 4.30: energy density plots for different stationary states in a condensate(having $\lambda_1 = 0$), plotted against ζ

4.6.3 Energy density plot for condensate having $\lambda_1 < 0$

In this part, we will look at the energy density plots for the ground state candidates (F1, F2, PM, and Polar) of a spinor BEC in a harmonic confinement having $\lambda_1 < 0$. Our system is already described in Section 4.4. Additionally, we fix $p' = 0.03$, $q' = 0.2$ and $N = 5000$.

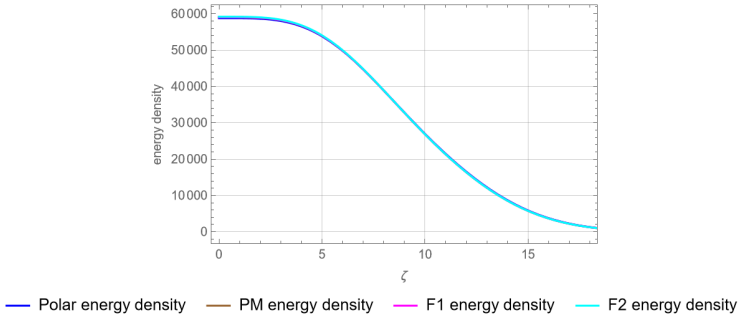

(a) energy density plots for different stationary states in a condensate (having $\lambda_1 < 0$), plotted against ζ, where $\zeta = 0$ is the 1-D trap center

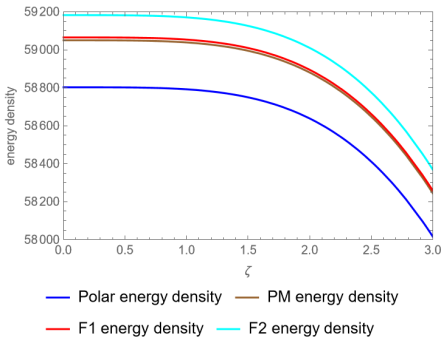

(b) energy density plots between $\zeta = 0$ to $\zeta = 3$, to clearly differentiate the energy densities of different stationary states

Figure 4.31: Energy density plots for $\lambda_1 < 0$

4.7 Discussion

This thesis introduces a variational method that helps us estimate the density functions for ground states of a trapped Spin-1 Bose-Einstein Condensate with fixed p(or p'), q(or q'), and N. Next, we saw that the number density profile found from our variational method matches quite well with numerical simulations [17] results. Subsequently, we looked at the phase boundaries for trapped systems. For condensates with $c_1 > 0$, we found a scaling factor dependent on N, which helps us move beyond the Thomas-Fermi approximations (which shows it to be independent of N). Furthermore, an interesting observation was that the Antiferromagnetic (AF)-Ferromagnetic phase boundary was a linear curve and is different from what was predicted by the homogeneous results(predicts it to be a constant curve). We also noticed that maintaining the same scaling factor could collapse all the phase boundaries to get a universal phase diagram irrespective of N. We also looked at condensates having $c_1 = 0$. Finally, we looked at condensates having $c_1 < 0$, where we realized the need to find the Ferromagnetic-Polar phase boundary, which was absent from Homogeneous results. We also saw a scaling factor to get a universal phase boundary for trapped condensates. Additionally, we examined the energy density plots for the ground state candidates of trapped condensates with different types of spin interactions.

Chapter 5

Conclusion and Outlook

5.1 Major Achievements

In this section, all the major findings are summarized.

- As we discussed, the T-F approximation omits the contribution from kinetic energy completely. Although this situation works perfectly well for large condensates, even for large condensates, there could arise a situation when the difference of energy between competing ground states would be so minimal that the Thomas-Fermi approximation will fail. Even for smaller condensates, the Thomas-Fermi approximation is known to be unreliable. Chapter 3 examined a variational method that considered kinetic energy contribution and achieved accurate results. This Variational method will even work irrespective of the values of N.

- This Variational method plays a crucial role in analytically obtaining the phase diagram of a condensate present in a generic trapping potential that wasn't possible previously. We also saw how the phase boundaries looked for Condensates having $c_1 > 0$, $c_1 = 0$ and $c_1 < 0$ present in a quasi 1-D harmonic confinement.

- For $c_1 > 0$, while finding the phase boundary, we realized that the Antiferromagnetic(AF)-Ferromagnetic phase boundary is linear, different from what was shown in the homogeneous results. We also learned that by applying the same scaling factor to the p', q' axis, we could achieve a universal phase boundary irrespective of the values of N. Furthermore, the scaling factor depends on N, highlighting the need to move beyond Thomas-Fermi approximations.

- For $c_1 < 0$, while finding the phase boundary, we realized the need to find the Polar-Ferromagnetic phase boundary, which was absent in the homogeneous results. We also learned that by applying the same scaling factor to the p', q' axis, we could achieve a universal phase boundary irrespective of the values of N.

5.2 Future Prospects

- As we discussed, our Variational method would be crucial in determining the phase boundary of a condensate in a generic trapping potential. So, from here on, one can analyze phase transitions for a trapped condensate as we now know the exact location of the phase boundary.
- In this thesis, we applied our Variational method for a condensate present in a 1-D trap. One can extend this variational method to higher dimensional space(In higher dimensional space, as we know, numerical analysis is computationally costly) and higher spin systems to find the phase boundaries.
- The variational method assumes that the phase part of the condensate wave function for individual spin components is either constant over space or slowly changing over space, effectively rejecting the spatial derivatives of the phase terms. We can generalize this method even further than the space-dependence of the phases to make it even more accurate. If successful, We can expect that this generalization would also make the method capable of getting to the vortex solutions, which was impossible with the previous scheme.
- An interesting direction would be investigating the transition to an excited state as we now have an idea about the ground state, e.g., we can look into the macroscopic tunneling phenomenon

Bibliography

[1] M. H. Anderson, J. R. Ensher, M. R. Matthews, C. E. Wieman, and E. A. Cornell. Observation of bose-einstein condensation in a dilute atomic vapor. *Science*, 269(5221):198–201, Jul 1995. URL: https://www.science.org/doi/10.1126/science.269.5221.198, doi:10.1126/science.269.5221.198.

[2] A. Aspect, E. Arimondo, R. Kaiser, N. Vansteenkiste, and C. Cohen-Tannoudji. Laser cooling below the one-photon recoil energy by velocity-selective coherent population trapping. *Phys. Rev. Lett.*, 61:826–829, Aug 1988. URL: https://link.aps.org/doi/10.1103/PhysRevLett.61.826, doi:10.1103/PhysRevLett.61.826.

[3] N. N. Bogolyubov. On the Theory of Superfluidity. *J. Phys. (USSR)*, 11:23–32, 1947. URL: https://www.ufn.ru/dates/pdf/j_phys_ussr/j_phys_ussr_1947_11_1/3_bogolubov_j_phys_ussr_1947_11_1_23.pdf.

[4] Satyendra Nath Bose. Plancks gesetz und lichtquantenhypothese. *Zeitschrift für Physik*, 26(1):178–181, 1924. doi:10.1007/BF01327326.

[5] C. C. Bradley, C. A. Sackett, J. J. Tollett, and R. G. Hulet. Evidence of bose-einstein condensation in an atomic gas with attractive interactions. *Phys. Rev. Lett.*, 75:1687–1690, Aug 1995. URL: https://link.aps.org/doi/10.1103/PhysRevLett.75.1687, doi:10.1103/PhysRevLett.75.1687.

[6] K. B. Davis, M. O. Mewes, M. R. Andrews, N. J. van Druten, D. S. Durfee, D. M. Kurn, and W. Ketterle. Bose-einstein condensation in a gas of sodium atoms. *Phys. Rev. Lett.*, 75:3969–3973, Nov 1995. URL: https://link.aps.org/doi/10.1103/PhysRevLett.75.3969, doi:10.1103/PhysRevLett.75.3969.

[7] A. Einstein. Quantentheorie des einatomigen idealen gases. zweite abhandlung. In *John Wiley & Sons, Ltd*, pages 245–257. John Wiley & Sons, Ltd, 2005. URL: https://onlinelibrary.wiley.com/doi/abs/10.1002/3527608958.ch28, doi:10.1002/3527608958.ch28.

[8] J. R. Ensher, D. S. Jin, M. R. Matthews, C. E. Wieman, and E. A. Cornell. Bose-einstein condensation in a dilute gas: Measurement of energy and ground-state occupation. *Phys. Rev. Lett.*, 77:4984–4987, Dec 1996. URL: https://link.aps.org/doi/10.1103/PhysRevLett.77.4984, doi:10.1103/PhysRevLett.77.4984.

[9] Fabrice Gerbier, Artur Widera, Simon Fölling, Olaf Mandel, and Immanuel Bloch. Resonant control of spin dynamics in ultracold quantum gases by microwave dressing. *Physical Review A*, 73(4), April 2006. URL: http://dx.doi.org/10.1103/PhysRevA.73.041602, doi:10.1103/physreva.73.041602.

[10] Eugene P Gross. Quantum theory of interacting bosons. *Annals of Physics*, 9(2):292–324, 1960. URL: https://www.sciencedirect.com/science/article/pii/0003491660900336, doi:10.1016/0003-4916(60)90033-6.

[11] Theodor Haensch and A.L. Schawlow. Hänsch, t. w. schawlow, a. l. cooling of gases by laser radiation. opt. commun. 13, 68-69. *Optics Communications*, 13:68–69, 01 1975. doi:10.1016/0030-4018(75)90159-5.

[12] Harald F. Hess, Greg P. Kochanski, John M. Doyle, Naoto Masuhara, Daniel Kleppner, and Thomas J. Greytak. Magnetic trapping of spin-polarized atomic hydrogen. *Phys. Rev. Lett.*, 59:672–675, Aug 1987. URL: https://link.aps.org/doi/10.1103/PhysRevLett.59.672, doi:10.1103/PhysRevLett.59.672.

[13] Projjwal K Kanjilal and A Bhattacharyay. Spin domains in ground state of a trapped spin-1 condensate: a general study under thomas–fermi approximation. *Physica Scripta*, 95(4):045702, feb 2020. URL: https://dx.doi.org/10.1088/1402-4896/ab5e95, doi:10.1088/1402-4896/ab5e95.

[14] Projjwal K Kanjilal and A Bhattacharyay. Multicomponent states for trapped spin-1 bose-einstein condensates in the presence of a magnetic field. *Physical Review A*, 108(5):053322, 2023. URL: https://link.aps.org/doi/10.1103/PhysRevA.108.053322.

[15] Projjwal Kanti Kanjilal and Arijit Bhattacharyay. A variational approach for the ground-state profile of a trapped spinor-bec: a detailed study of phase transition in spin-1 condensate at zero magnetic field. *The European Physical Journal Plus*, 137(5):547, 2022. URL: https://link.springer.com/article/10.1140/epjp/s13360-022-02729-0.

[16] Projjwal Kanti Kanjilal and ARIJIT Bhattacharyay. *Investigation of ground states of spin-1 Bose-Einstein condensate in a harmonic trap*. PhD thesis, Indian Institute of Science

Education and Research, Pune, 2023. URL: http://dr.iiserpune.ac.in:8080/xmlui/handle/123456789/8181.

[17] Pardeep Kaur, Arko Roy, and Sandeep Gautam. Fortress: Fortran programs for solving coupled gross–pitaevskii equations for spin–orbit coupled spin-1 bose–einstein condensate. *Computer Physics Communications*, 259:107671, 2021. URL: https://www.sciencedirect.com/science/article/pii/S001046552030326X, doi:10.1016/j.cpc.2020.107671.

[18] Yuki Kawaguchi and Masahito Ueda. Spinor bose–einstein condensates. *Physics Reports*, 520(5):253–381, 2012. Spinor Bose–Einstein condensates. URL: https://www.sciencedirect.com/science/article/pii/S0370157312002098, doi:10.1016/j.physrep.2012.07.005.

[19] W. Ketterle, M. R. Andrews, K. B. Davis, D. S. Durfee, D. M. Kurn, M.-O. Mewes, and N. J. van Druten. Bose–einstein condensation of ultracold atomic gases. *Physica Scripta*, 1996(T66):31, 1996. URL: https://dx.doi.org/10.1088/0031-8949/1996/T66/004, doi:10.1088/0031-8949/1996/T66/004.

[20] S. R. Leslie, J. Guzman, M. Vengalattore, Jay D. Sau, Marvin L. Cohen, and D. M. Stamper-Kurn. Amplification of fluctuations in a spinor bose-einstein condensate. *Physical Review A*, 79(4), April 2009. URL: http://dx.doi.org/10.1103/PhysRevA.79.043631, doi:10.1103/physreva.79.043631.

[21] F. London. On the bose-einstein condensation. *Phys. Rev.*, 54:947–954, Dec 1938. URL: https://link.aps.org/doi/10.1103/PhysRev.54.947, doi:10.1103/PhysRev.54.947.

[22] Naoto Masuhara, John M. Doyle, Jon C. Sandberg, Daniel Kleppner, Thomas J. Greytak, Harald F. Hess, and Greg P. Kochanski. Evaporative cooling of spin-polarized atomic hydrogen. *Phys. Rev. Lett.*, 61:935–938, Aug 1988. URL: https://link.aps.org/doi/10.1103/PhysRevLett.61.935, doi:10.1103/PhysRevLett.61.935.

[23] PITAEVSKII L. P. Vortex lines in an imperfect bose gas. *Sov. Phys.-JETP*, 13(2):451, 1961. URL: https://cir.nii.ac.jp/crid/1571698599883889664.

[24] Oliver Penrose and Lars Onsager. Bose-einstein condensation and liquid helium. *Phys. Rev.*, 104:576–584, Nov 1956. URL: https://link.aps.org/doi/10.1103/PhysRev.104.576, doi:10.1103/PhysRev.104.576.

[25] D. M. Stamper-Kurn, M. R. Andrews, A. P. Chikkatur, S. Inouye, H.-J. Miesner, J. Stenger, and W. Ketterle. Optical confinement of a bose-einstein condensate. *Phys. Rev. Lett.*, 80:2027–2030, Mar 1998. URL: https://link.aps.org/doi/10.1103/PhysRevLett.80.2027, doi:10.1103/PhysRevLett.80.2027.

[26] D. M. Stamper-Kurn and W. Ketterle. *Spinor Condensates and Light Scattering from Bose-Einstein Condensates*, page 139–217. Springer Berlin Heidelberg. URL: http://dx.doi.org/10.1007/3-540-45338-5_2, doi:10.1007/3-540-45338-5_2.

[27] Dan M. Stamper-Kurn and Masahito Ueda. Spinor bose gases: Symmetries, magnetism, and quantum dynamics. *Rev. Mod. Phys.*, 85:1191–1244, Jul 2013. URL: https://link.aps.org/doi/10.1103/RevModPhys.85.1191, doi:10.1103/RevModPhys.85.1191.

[28] Simon Stellmer, Benjamin Pasquiou, Rudolf Grimm, and Florian Schreck. Laser cooling to quantum degeneracy. *Phys. Rev. Lett.*, 110:263003, Jun 2013. URL: https://link.aps.org/doi/10.1103/PhysRevLett.110.263003, doi:10.1103/PhysRevLett.110.263003.

[29] Boyuan Wang. Review on bose-einstein condensation. *Highlights in Science, Engineering and Technology*, 38:19–29, 03 2023. doi:10.54097/hset.v38i.5689.